nature geoscience

ARTICLES

https://doi.org/10.1038/s41561-021-00692-6

Calibrating the marine turbidite palaeoseismometer using the 2016 Kaikōura earthquake

Jamie D. Howarth[1]✉, Alan R. Orpin[2], Yoshihiro Kaneko[3,4], Lorna J. Strachan[5], Scott D. Nodder[2], Joshu J. Mountjoy[2], Philip M. Barnes[2], Helen C. Bostock[2,6], Caroline Holden[3], Katie Jones[1] and M. Namik Cağatay[7]

Turbidite palaeoseismology has produced arguably the most comprehensive multimillennial scale records of subduction-zone earthquakes but is underpinned by techniques that are vigorously debated in earthquake science. Resolving this argument requires new direct observations that test the approach's essential assumptions. Here we present measurements from turbidites triggered by the 2016 M_w 7.8 Kaikōura earthquake in New Zealand, one of the most well-instrumented earthquakes in history. This natural experiment provides an ideal test for turbidite palaeoseismology because fault source, ground motions and turbidite deposition in discrete canyons are well-resolved by analysis of sediment cores combined with physics-based ground-motion modelling. We find that the Kaikōura earthquake triggered flows in ten consecutive canyon–distributary systems along a 200 km segment of the Hikurangi subduction margin where long-period (>2 s) peak ground velocities exceeded turbidity-current-triggering thresholds between 16–25 cm s^{-1}. Comparison between ground motions and turbidite deposition confirm that there is a predictable relationship between earthquake source, ground motions and deposition of coseismic turbidites. We demonstrate that the patterns of triggering and resultant turbidite character may preserve evidence of fault-rupture direction along with the radiating patterns and amplification of earthquake ground motions.

Subduction zones generate the largest and most damaging earthquakes on Earth[1,2], but the dynamics of these faults and the hazard they pose is poorly understood due to the paucity of high-resolution earthquake records that span millennia[1,3,4]. Deep-sea turbidites can offer the longest and most spatially complete records of subduction-zone earthquakes[5–9]. Despite a growing number of turbidite palaeoseismology studies[5,7,8,10–14], vigorous debate persists[14–21] regarding the validity of the assumptions that underpin this approach[6,22]. These are: (1) there is a predictable relationship between the earthquake source, strong ground motions (SGM) and synchronously triggered turbidity currents in discrete sediment dispersal systems along the length of ruptured subduction zones, potentially eliminating more localized triggers such as storm waves, tides or floods, and (2) synchronicity can be established retrospectively from sedimentological and geochronological studies of sediment cores. With numerical dating techniques currently limited by decadal uncertainties, turbidite palaeoseismologists often use two relative dating techniques to infer synchronicity: 'turbidite fingerprinting' and the 'confluence test' (Fig. 1c). A rigorous test of the two main assumptions underpinning turbidite palaeoseismology remains elusive because it requires measurement of three criteria: the fault rupture, the spatial distribution of SGMs produced by the earthquake and spatially extensive sampling of resultant coseismic turbidites. While previous studies have identified recent turbidites triggered by earthquakes[5,23–25], high-resolution datasets that meet all three criteria for testing turbidite palaeoseismology are unprecedented. We use sediment cores from along the southern Hikurangi subduction margin (HSM), New Zealand, to identify coseismic turbidites triggered by the 2016 moment magnitude (M_w) 7.8 Kaikōura earthquake. Collectively, these provide a rigorous test of the turbidite palaeoseismology approach.

Rupture geometry and slip distribution for the 2016 Kaikōura earthquake are among the most well-constrained historically through a combination of geodesy[26], seismology[27] and field-mapping[28] (Fig. 1a). The earthquake ruptured 21 onshore and offshore faults in an ~180-km-long zone of the northeastern South Island[28]. Physics-based models of earthquake ground motion are well corroborated by both near- and far-field station data[29] and show that SGMs propagated along much of the southern HSM[29–31]. The spatial distribution of large aftershocks was generally limited to onshore locations proximal to fault ruptures[32] (Fig. 1b). Offshore ground motions produced by even the largest aftershocks were minimal compared with the mainshock, facilitating robust temporal correlations between the M_w 7.8 2016 Kaikōura earthquake and offshore turbidites triggered by the event (Supplementary Fig. 1). Post-earthquake sea-floor mapping and sediment coring demonstrated that the earthquake caused widespread submarine landsliding and triggered a turbidity current that travelled >680 km along the Hikurangi Channel[33] (Fig. 1a). The submarine sedimentary distributary systems that feed the Hikurangi Channel are characterized by multiple feeder canyons that incise the continental shelf both parallel and perpendicular to the fault rupture, providing an ideal orientation for testing turbidite palaeoseismology (Fig. 1b).

Turbidite structure and spatial distribution

The spatial distribution of turbidite deposition resulting from the 2016 Kaikōura earthquake was determined using a total of 31

[1]School of Geography, Environment and Earth Sciences, Victoria University of Wellington, Wellington, New Zealand. [2]National Institute of Water and Atmospheric Research (NIWA), Wellington, New Zealand. [3]GNS Science, Lower Hutt, New Zealand. [4]Graduate School of Science, Kyoto University, Kyoto, Japan. [5]School of Environment, University of Auckland, Auckland, New Zealand. [6]School of Earth and Environmental Sciences, University of Queensland, Brisbane, Queensland, Australia. [7]EMCOL Research Centre and Department of Geological Engineering, Istanbul Technical University, Istanbul, Turkey. ✉e-mail: jamie.howarth@vuw.ac.nz

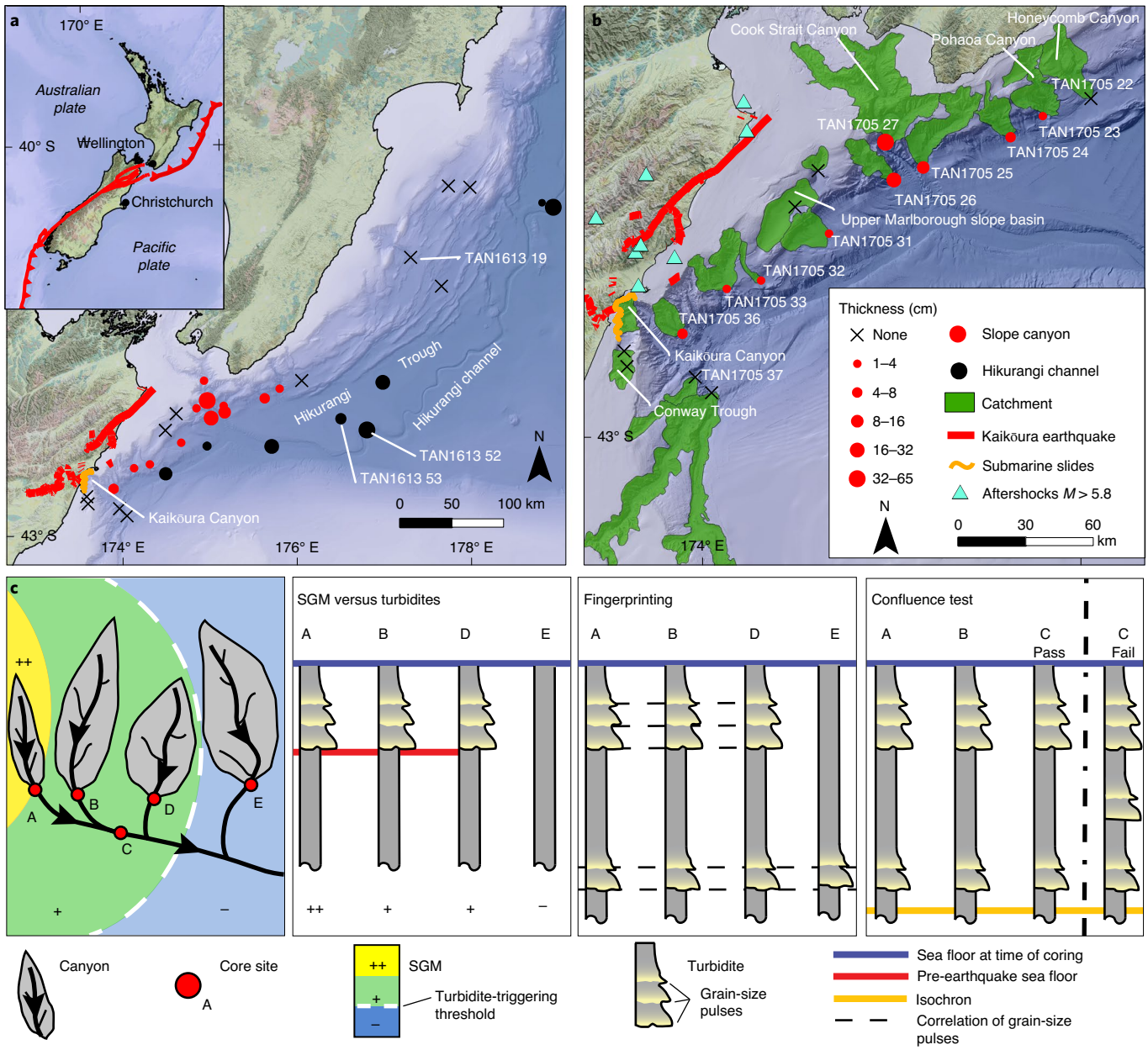

Fig. 1 | Tectonic setting and post-earthquake sample sites along the southern HSM and schematics of the assumptions that underpin turbidite palaeoseismology. a, 2016 Kaikōura earthquake fault ruptures (red lines), the spatial distribution and thickness of all coseismic turbidites along the HSM (red dots for cores sampling discrete canyons and black dots for cores that capture turbidites from the long-run-out turbidity current that traversed the Hikurangi Channel[33]) and mapped submarine landslides (orange line)[33]. Inset: New Zealand's tectonic setting. **b**, Turbidite thickness and upstream catchment area (green polygons) for the discrete sediment distributary systems sampled during the coring campaign. **c**, Schematic of the conceptual tests that underpin the main assumptions for turbidite palaeoseismology including (from left to right): the relationship between SGM (++ denotes the strongest shaking) and turbidite triggering, application of turbidite fingerprinting and application of the confluence test. Turbidite 'fingerprinting' has been used to make arguments of synchronicity at locations where it is not possible to use the confluence test[5,9], based on observations that some turbidites with the same age distributions from different canyons have similar patterns of grain-size pulsing. The confluence test uses counts of turbidites between temporal datums above and below the confluence of major submarine channels/canyons[6,9,42]. At appropriate length scales, flows triggered synchronously in separate canyon heads are assumed to produce a single turbidite above and below the confluence of the distributary system. In contrast, asynchronous flows will be additive, producing one deposit in each channel above the confluence and more than one in the channel below.

sediment cores collected during 2 campaigns that occurred 3 days (voyage TAN1613) and 8 months (TAN1705) after the earthquake (Fig. 1a). These cores sampled 20 discrete canyon or slope-basin catchments along 700 km of the southern and central HSM. Core sites were located to an accuracy of <10 m and positioned on the canyon cross-section to maximize preservation of turbidites and avoid erosion features (Methods; Supplementary Table 1; Supplementary Figs. 2–13).

The presence/absence of 2016 Kaikōura earthquake turbidites was inferred using a combination of short-lived radioisotope dating (^{234}Th, ^{210}Pb) and lithological indicators of recent deposition, such as lack of bioturbation, an underlying oxic layer indicative of recent

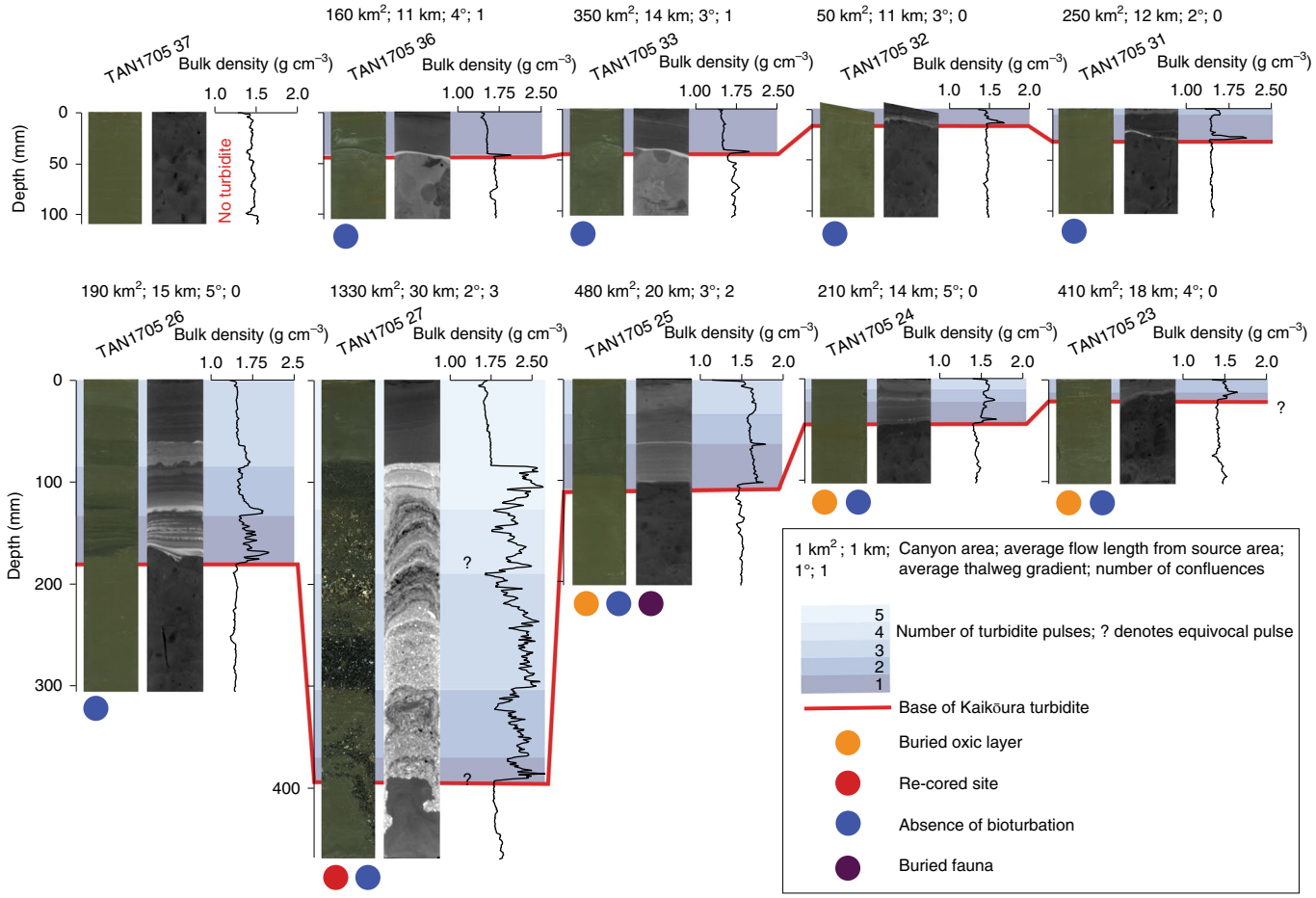

Fig. 2 | Kaikōura earthquake turbidites from canyons on the southern HSM. Core imagery, CT scans and plots of bulk density are shown for sites from SW (top left) to NE (lower right) along the margin. The number of grain-size pulses recorded by down-core density profiles varies along the margin with one pulse in the three SW canyons and multiple pulses in the NE (Fig. 1 shows the locations).

surficial sea floor and freshly buried biological remains[33] (Fig. 2; Supplementary Figs. 14 and 15; Supplementary Discussion 1). Coseismic turbidites have an average thickness of ~100 mm but are highly variable (20–650 mm, Fig. 2). The turbidites are characterized by one or more grain-size pulses. Here, we define a grain-size pulse as a discrete, normally graded interval, generally characterized by planar, laminated, very fine sandy silts (T_D) overlain by normally graded mud (T_{E-1} or T_{E-2})[34–36]. These grain-size pulses are also resolved in core imagery and high-resolution down-core density profiles produced by computed tomography (CT), which provide a proxy for mean grain size (Supplementary Fig. 16). Coseismic turbidites in cores from the three SW canyons have a single grain-size pulse (TAN1705 36, 33 and 32), while cores from the NE canyons typically have multiple pulses (TAN1705 31, 26, 27, 25, 24 and 23) (Fig. 2; Supplementary Discussion 2). Turbidites with a single grain-size pulse are interpreted to have formed by a turbidity current with waning velocity over time, while those with more than one grain-size pulse were produced by turbidity currents with multiple velocity surges[34,37].

In two cores, the exact number of grain-size pulses preserved is less certain (Fig. 2). The turbidite (TAN1705 23) at the northernmost extent of triggering is only 20 mm thick and it is unclear whether it has one or two grain-size pulses. Similarly, distinguishing individual grain-size pulses in the basal section of the Cook Strait canyon turbidite (TAN1705 27) is also problematic due to its very coarse sand–gravel texture with shell hash. We interpret three to five normally graded bands are present from the high-resolution core image and density profile to acknowledge the high degree of uncertainty in the definition of grain-size pulses (Fig. 2; Supplementary Discussion 2).

Coseismic triggering of turbidity currents by the 2016 Kaikōura earthquake was identified in ten consecutive canyons along a >200 km segment of the margin (Fig. 3). The NE and SW extents of triggering occur 120 km north of the rupture tip between the Pahaoa and Honeycomb canyons and 15 km SE of the southern extent of rupture in the Conway trough, respectively (Fig. 3). Triggering is interrupted along strike by the absence of turbidites in cores from the upper Marlborough slope basin (TAN1613 60 and TAN1705 40; Fig. 3). An explanation for this absence could be the older age and greater consolidation of sediment sources exposed in the gully heads of the distributary system. There, sea-floor samples and sediment thicknesses estimated from sub-bottom profiles reveal partly lithified mid-Pleistocene or older units outcropping at the sea floor, and little to no postglacial (<20 thousand years ago) deposition on the outermost shelf[38] (Supplementary Fig. 20). We infer that these characteristics make this locality less sensitive to seismic shaking and turbidity-current triggering, and therefore do not consider it further in our analysis.

Correlating turbidites with ground motions

To qualify the relationship between the spatial pattern of shaking from the 2016 Kaikōura earthquake and turbidite deposition, we perform physics-based ground-motion simulations of the earthquake. Simulations are based on a published fault-source model[29]

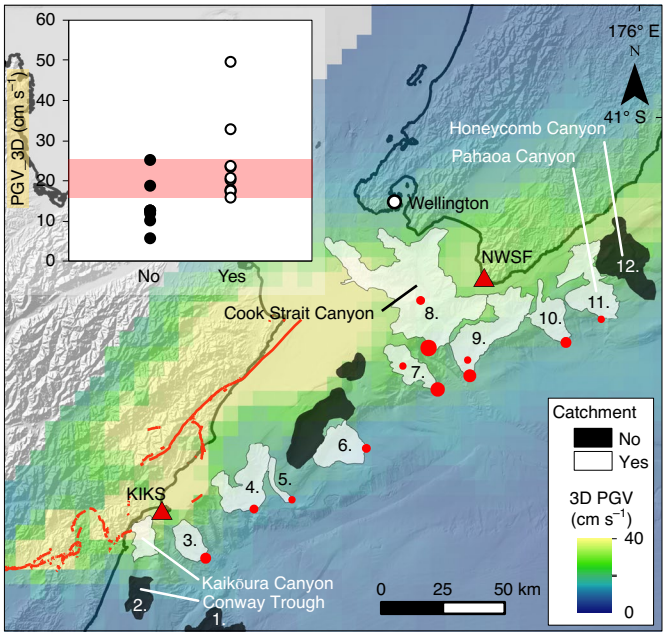

Fig. 3 | The relationship between fault source, ground motions and coseismic turbidites. The spatial distribution of PGV (from the 3D velocity model) and turbidite deposition. Inset: populations of PGVs for turbidite triggering (Yes) and no triggering (No) used to derive the range of triggering thresholds. Catchment numbers 1 through 12 refer to the relevant seismograms in Fig. 4.

and account for both three-dimensional (3D) velocity and attenuation models for New Zealand (Methods). Modelled ground motions are expressed in terms of their magnitude of surface velocity calculated up to 0.5 Hz and are validated against onshore seismic and geodetic data along the HSM[30] (Supplementary Fig. 17).

Modelled PGVs are highest nearest the rupture tip and to the NE, due to the directionality of rupture and amplification of motions in the low-velocity subduction-zone sedimentary prism[30]. We find that the radiating pattern of seismic energy along the rupture and northwards of its tip is well reflected by the spatial pattern of turbidity-current triggering in canyons (Fig. 3). Comparison of PGV between canyons that record turbidites with those that did not indicate threshold PGVs for triggering turbidity currents ranged from 16–25 cm s^{-1}. The specific PGV threshold depends on the assumed velocity model, but this spatial pattern of PGVs and triggering is retained in simulations with different velocity models (Supplementary Fig. 18).

Validation of turbidite palaeoseismology

We have shown that coseismic turbidites were deposited near synchronously in discrete canyons along a substantial spatial extent of the southern HSM and that this spatial distribution correlates with ground motions modelled from the fault source. These observations support one of the main underpinning assumptions of turbidite palaeoseismology that has been widely debated[14,15,19,21]: that is, there is a predictable relationship between the earthquake source, the spatial distribution of SGM, synchronous triggering of turbidity currents and emplacement of coseismic turbidites in discrete canyon–distributary systems along subduction margins. Moreover, these data now enable us to evaluate one of the methodologies commonly used to infer synchronicity of triggering retrospectively from sediment cores[13,24].

Turbidite 'fingerprinting' has been used to make arguments of synchronous triggering of turbidity currents based on observations that some turbidites with the same age distributions from different canyons have similar patterns of grain-size pulsing[5,9,34] (Fig. 1c). Multipulsed turbidites in discrete canyons separated by along-margin distances of up to 1,000 km have been correlated with, and are inferred to result from, flows sharing the same number of velocity surges, each relating to an episode of canyon-head mass wasting[9]. Proponents have argued that common ground-motion time histories across many canyons from a large earthquake is the only process capable of causing simultaneous triggering of multiple phases of canyon-head mass wasting and in turn, multiple velocity surges in turbidity currents over such large distances[5,9,34]. Our study provides an opportunity to test this conceptual model through direct comparison of the ground-motion time history of the earthquake with the sedimentary structure of earthquake-triggered turbidites.

Ground-velocity time histories from the 2016 Kaikōura earthquake recorded by the SGM stations nearest the southernmost (site KIKS) and northernmost (site NTWS) canyons show an increasing number of prominent amplitude peaks (defined here as >50% of the maximum amplitude) from SW to NE (Fig. 4a). This spatial pattern of velocity amplitude peaks is mirrored by the shift from single- to multipulse turbidites (Fig. 2), indicating that multiple high-velocity amplitude peaks may have caused multiphased canyon-head mass wasting, surges in flow and resultant multipulsed turbidite deposits.

To explore this relationship between SGM and turbidite structure further, we use the ground-motion simulation to extract the ground-velocity time history of the 2016 Kaikōura earthquake for the centroid of each canyon catchment (Fig. 4b). As the specific ground-motion-triggering threshold for each catchment remains unknown, it is not possible to directly compare the number of grain-size pulses and velocity amplitude peaks above that threshold. Instead, we use a simple pass/fail criteria that accounts for the range of potential triggering thresholds (Methods). A regional comparison shows that only a single velocity amplitude peak reaches the triggering threshold range of 16–25 cm s^{-1} in the three SW canyons, all of which produced turbidites with a single grain-size pulse (TAN1705 32, 33 and 36). Similarly, multiple velocity amplitude peaks reach the range of triggering thresholds in canyons that produced matching multipulsed turbidites (TAN1705 23, 24, 25, 26, 27 and 31; Fig. 4b). Only one site out of nine canyons that have the 2016 Kaikōura turbidite failed our agreement criteria (TAN1705 24), but even this core retains multiple grain-size pulses and occurs in a catchment with multiple velocity amplitude peaks that reach the triggering threshold range (Fig. 4b). These observations are consistent with a relationship between earthquake ground motions and grain-size multipulses in earthquake-triggered turbidites. However, other explanations are potentially important.

Non-seismic processes that can influence the number of grain-size pulses preserved in turbidites include downstream merging of flow-velocity surges[39,40], amalgamation of flows downstream of confluences[37] and erosion of a deposit by subsequent velocity surges[9,41]. Flume experiments show that multiple phases of mass wasting propagate discrete surges in turbidity currents, but those surging flows tend to merge downstream[37,39,40]. Upscaling from the flume to natural canyons infers that merging might occur a few tens of kilometres downstream from source areas[39], which is the same length scale as the average flow path from source areas in many of the distributary canyons from the southern HSM (Supplementary Fig. 19). To assess whether the along-margin spatial distribution of pulses observed in the 2016 Kaikōura turbidite could be attributed to downstream merging of velocity surges, we conducted a morphometric analysis of the distributary canyons. Source area, average flow-path distance from source areas, thalweg gradients and the number of major confluences within each distributary canyon are broadly consistent across five of the nine canyons (TAN1705 36, 33, 26, 25 and 24). These canyons also span the SW to NE spatial distribution of coseismic turbidite occurrence and preserved both single- and

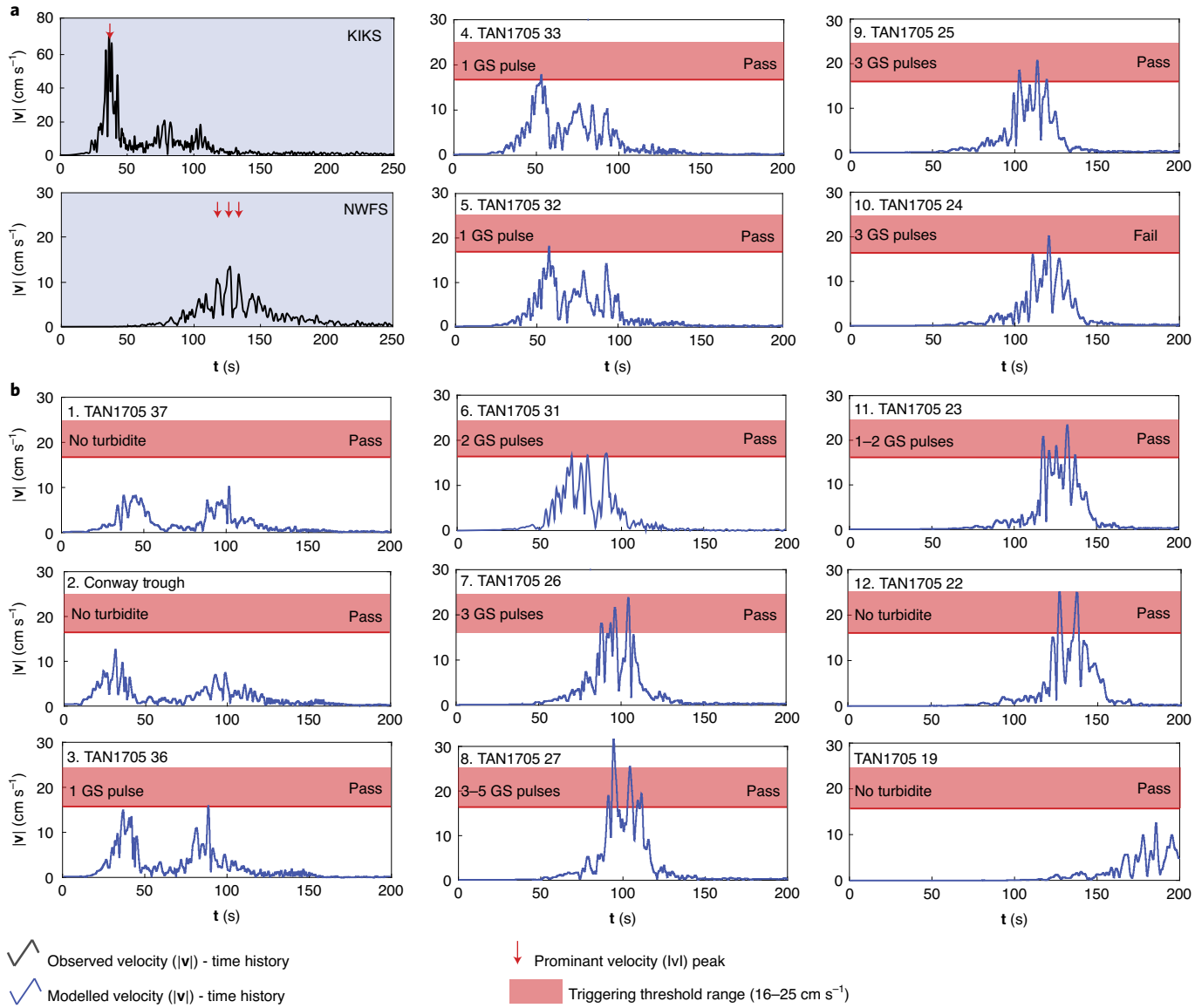

Fig. 4 | Comparison between grain-size pulses in coseismic turbidites and seismograms of the triggering earthquake. a, The closest strong-motion stations to the southern and northern canyons (KIKS and NWFS stations, respectively) show an increase from a single to multiple prominent ground velocity (|**v**|) amplitude peaks from SW to NE along the margin, which is similar to the pattern of grain-size pulses observed in coseismic turbidites. **b**, Comparison between the number of amplitude peaks in synthetic velocity time (t) histories (blue) and grain-size (GS) pulses in turbidites. Numbers refer to canyon locations in Fig. 3. Pass: sites that pass the comparison test between ground-velocity amplitude peaks and grain-size pulses in turbidites are those where the number of velocity peaks with amplitudes within the regional triggering-threshold range (16–25 cm s^{-1}) was greater than or equal to the number of grain-size pulses in the turbidite. Fail: sites fail the comparison when either (1) the number of grain-size pulses exceeded the number of velocity peaks that reach the triggering-threshold range; or (2) fewer grain-size pulses were observed than the number of velocity peaks exceeding the upper bound of the triggering-threshold range (that is, 25 cm s^{-1}).

multipulse turbidites. Consequently, advocating for downstream merging of flow-velocity surges to explain the single-pulse turbidites in the SW canyons is not justified while simultaneously arguing that merging has not occurred in the NE canyons, several of which have longer flow-path distances from source. Similar arguments can be made for flow amalgamation downstream of confluences because the number of confluences per canyon does not scale with the number of grain-size pulses. We cannot rule out complete removal of grain-size pulses by erosion during the turbidity currents, though this scenario is mitigated to some degree by core-site locations[9] and the observation that some turbidites conformably overlie undisturbed oxic sea-floor sediments.

We surmise that while our observations and modelling are not a definitive test of the relationship between earthquake ground motions and turbidite characteristics, they do provide strong evidence that, at appropriate length scales, turbidite structures may preserve elements of the seismogram of the triggering earthquake. However, the spatial variation in ground-motion time histories for a given event may make application of the 'fingerprinting' approach for correlating turbidites challenging. For example, if the suite of coseismic turbidites triggered by the 2016 Kaikōura earthquake occurred in the geologic record, we contend that the dual fingerprints of single- versus multipulse turbidites would probably be misinterpreted as two separate earthquakes.

The confluence test is the other approach used by turbidite palaeoseismologists to generate arguments of synchronous triggering of turbidites in the sedimentary record. Our study does not provide the means to evaluate the confluence test because that would require the number of turbidites to be counted between two temporal datums above and below the confluence of submarine channels/canyons[6,9,42] (Fig. 1c). However, we do show that the 2016 Kaikōura earthquake emplaced a single turbidite above and below major canyon/channel confluences (Supplementary Fig. 20). Should underlying turbidites deposited by historical earthquakes (for example, the 1855 M_w 8.2 Wairarapa earthquake[43]) be identified with radiometric dating at these and other core sites along canyon axis cross-sections then the southern Hikurangi margin will provide an ideal location to assess the confluence test using known earthquakes. Elements of this work now form the basis of ongoing research programmes.

Implications for turbidite palaeoseismology

The 2016 Kaikōura earthquake case study provides the first comprehensive evidence that there is a predictable relationship between fault source, rupture direction, ground motions and the spatial distribution of coseismic turbidites. However, the observed relationships between these variables raise some important issues and opportunities. This study illustrates that not all coseismic turbidites on subduction margins owe their origin to plate-interface ruptures, emphasizing the need to evaluate upper-plate earthquake sources in regional palaeoseismic investigations[44,45]. Furthermore, the study demonstrates that using the spatial distribution of turbidites as a proxy for rupture length and earthquake magnitude may be complicated by the asymmetric radiation of ground motions from a specific fault source. The observed asymmetry is caused by a combination of rupture direction and the radiating patterns and amplification of earthquake ground motions in the low-velocity sedimentary prism[30]; physical attributes that are common on subduction zones globally. Rather than being a limitation, the nuanced relationship between fault rupture, the spatial distribution of ground motions and turbidite triggering offers the potential to resolve earthquake rupture direction in palaeoseismic events constrained by additional proxies, such as rupture length from on-fault or coastal-vertical-deformation palaeoseismology. The potential of coseismic turbidites to provide a proxy for rupture direction is an important breakthrough as it is an essential parameter for accurately quantifying ground-motion hazard[46], but is difficult to reconstruct for prehistoric earthquakes[47].

The apparent relationship between earthquake ground-motion time histories and grain-size pulses in the observed coseismic turbidites make it plausible that prehistoric coseismic turbidites could be natural seismometers. Despite compelling experimental studies, uncertainties remain about the failure mechanism[48] and flow processes that allow such signatures to be preserved in flows[40]. However, one plausible though speculative explanation is rapid, retrogressive shallow submarine landsliding during which dynamic displacements associated with ground-motion amplitude peaks cause repeated episodes of failure in unconsolidated, weak, muddy sediment during the shaking period[49] (Supplementary Discussion 3). To further test whether turbidite structure can be used to reconstruct the seismograms from palaeo-earthquakes, future observational studies are needed to better constrain local ground motions, morphological changes at source areas and site-specific heterogeneity in turbidite character. If substantiated, turbidite records could ultimately advance our ability to identify asperities on subduction-zone faults, estimate rupture direction and help to qualify spatial variation in ground motions.

Online content

Any methods, additional references, Nature Research reporting summaries, source data, extended data, supplementary information, acknowledgements, peer review information; details of author contributions and competing interests; and statements of data and code availability are available at https://doi.org/10.1038/s41561-021-00692-6.

Received: 7 February 2020; Accepted: 6 January 2021;
Published online: 04 March 2021

References

1. Simons, M. et al. The 2011 magnitude 9.0 Tohoku-Oki earthquake: mosaicking the megathrust from seconds to centuries. *Science* **332**, 1421–1425 (2011).
2. Bilek, S. L. & Lay, T. Subduction zone megathrust earthquakes. *Geosphere* **14**, 1468–1500 (2018).
3. Normile, D. Scientific consensus on great quake came too late. *Science* **332**, 22–23 (2011).
4. Sieh, K. et al. Earthquake supercycles inferred from sea-level changes recorded in the corals of West Sumatra. *Science* **322**, 1674–1678 (2008).
5. Patton, J. R. et al. A 6600 year earthquake history in the region of the 2004 Sumatra-Andaman subduction zone earthquake. *Geosphere* **11**, 2067–2129 (2015).
6. Goldfinger, C. Submarine paleoseismology based on turbidite records. *Ann. Rev. Mar. Sci.* **3**, 35–66 (2011).
7. Moernaut, J. et al. Larger earthquakes recur more periodically: new insights in the megathrust earthquake cycle from lacustrine turbidite records in south-central Chile. *Earth Planet. Sci. Lett.* **481**, 9–19 (2018).
8. Moernaut, J. et al. Lacustrine turbidites as a tool for quantitative earthquake reconstruction: new evidence for a variable rupture mode in south central Chile. *J. Geophys. Res. Solid Earth* **119**, 1607–1633 (2014).
9. Goldfinger, C. et al. *Turbidite Event History—Methods and Implications for Holocene Paleoseismicity of the Cascadia Subduction Zone* Professional Paper No. 1661-F (USGS, 2012).
10. Howarth, J. D., Fitzsimons, S. J., Norris, R. J. & Jacobsen, G. E. Lake sediments record high intensity shaking that provides insight into the location and rupture length of large earthquakes on the Alpine Fault, New Zealand. *Earth Planet. Sci. Lett.* **403**, 340–351 (2014).
11. Howarth, J. D., Fitzsimons, S. J., Norris, R. J., Langridge, R. & Vandergoes, M. J. A 2000 yr rupture history for the Alpine Fault derived from Lake Ellery, South Island, New Zealand. *Geol. Soc. Am. Bull.* **128**, 627–643 (2016).
12. Goldfinger, C. et al. Late Holocene rupture of the northern San Andreas Fault and possible stress linkage to the Cascadia subduction zone. *Bull. Seismol. Soc. Am.* **98**, 861–889 (2008).
13. Gràcia, E. et al. Holocene earthquake record offshore Portugal (SW Iberia): testing turbidite paleoseismology in a slow-convergence margin. *Quat. Sci. Rev.* **29**, 1156–1172 (2010).
14. Goldfinger, C. et al. The importance of site selection, sediment supply, and hydrodynamics: a case study of submarine paleoseismology on the northern Cascadia margin, Washington USA. *Mar. Geol.* **384**, 4–46 (2017).
15. Goldfinger, C. et al. Can turbidites be used to reconstruct a paleoearthquake record for the central Sumatran margin?: COMMENT. *Geology* **42**, e344 (2014).
16. Goldfinger, C., Wong, I., Kulkarni, R. & Beeson, J. W. Reply to "Comment on 'Statistical analyses of great earthquake recurrence along the Cascadia subduction zone' by Ram Kulkarni, Ivan Wong, Judith Zachariasen, Chris Goldfinger, and Martin Lawrence" by Allan Goddard Lindh. *Bull. Seismol. Soc. Am.* **106**, 2935–2944 (2016).
17. Lindh, A. G. Comment on "Statistical analyses of great earthquake recurrence along the Cascadia subduction zone" by Ram Kulkarni, Ivan Wong, Judith Zachariasen, Chris Goldfinger, and Martin Lawrence. *Bull. Seismol. Soc. Am.* **106**, 2927–2934 (2016).
18. Shanmugam, G. Comment on "Late Holocene rupture of the northern San Andreas Fault and possible stress linkage to the Cascadia subduction zone" by Chris Goldfinger, Kelly Grijalva, Roland Bürgmann, Ann E. Morey, Joel E. Johnson, C. Hans Nelson, Julia Gutiérrez-Pastor, Andrew Ericsson, Eugene Karabanov, Jason D. Chaytor, Jason Patton, and Eulàlia Gràcia. *Bull. Seismol. Soc. Am.* **99**, 2594–2598 (2009).
19. Sumner, E. J. et al. Can turbidites be used to reconstruct a paleoearthquake record for the central Sumatran margin? *Geology* **41**, 763–766 (2013).
20. Talling, P. J. et al. Key future directions for research on turbidity currents and their deposits. *J. Sediment. Res.* **85**, 153–169 (2015).
21. Atwater, B. F., Carson, B., Griggs, G. B., Johnson, H. P. & Salmi, M. Rethinking turbidite paleoseismology along the Cascadia subduction zone. *Geology* **42**, 827–830 (2014).
22. Goldfinger, C. in *International Geophysics* Vol. 95 (ed. McCalpin, J. P.) Ch. 2B (Academic Press, 2009).
23. McHugh, C. M. et al. Offshore sedimentary effects of the 12 January 2010 Haiti earthquake. *Geology* **39**, 723–726 (2011).
24. Ikehara, K. et al. Documenting large earthquakes similar to the 2011 Tohoku-Oki earthquake from sediments deposited in the Japan Trench over the past 1500 years. *Earth Planet. Sci. Lett.* **445**, 48–56 (2016).

25. Van Daele, M. et al. A comparison of the sedimentary records of the 1960 and 2010 great Chilean earthquakes in 17 lakes: implications for quantitative lacustrine palaeoseismology. *Sedimentology* **62**, 1466–1496 (2015).
26. Hamling, I. J. et al. Complex multifault rupture during the 2016 M_w 7.8 Kaikōura earthquake, New Zealand. *Science* https://doi.org/10.1126/science.aam7194 (2017).
27. Kaiser, A. et al. The 2016 Kaikōura, New Zealand, earthquake: preliminary seismological report. *Seismol. Res. Lett.* **88**, 727–739 (2017).
28. Litchfield, N. J. et al. Surface rupture of multiple crustal faults in the 2016 M_w 7.8 Kaikōura, New Zealand, earthquake. *Bull. Seismol. Soc. Am.* **108**, 1496–1520 (2018).
29. Holden, C. et al. The 2016 Kaikōura earthquake revealed by kinematic source inversion and seismic wavefield simulations: slow rupture propagation on a geometrically complex crustal fault network. *Geophys. Res. Lett.* **44**, 11320–11328 (2017).
30. Wallace, L. M. et al. Large-scale dynamic triggering of shallow slow slip enhanced by overlying sedimentary wedge. *Nat. Geosci.* **10**, 765–770 (2017).
31. Bradley, B. A., Razafindrakoto, H. N. T. & Polak, V. Ground-motion observations from the 14 November 2016 M_w 7.8 Kaikōura, New Zealand, earthquake and insights from broadband simulations. *Seismol. Res. Lett.* **88**, 740–756 (2017).
32. Meng, Q., Ni, S., Guo, A. & Zhou, Y. Ground surface deformation caused by the M_w 5.8 early strong aftershock following the 13 November 2016 M_w 7.8 Kaikōura mainshock. *Seismol. Res. Lett.* **89**, 2214–2226 (2018).
33. Mountjoy, J. J. et al. Earthquakes drive large-scale submarine canyon development and sediment supply to deep-ocean basins. *Sci. Adv.* https://doi.org/10.1126/sciadv.aar3748 (2018).
34. Gutiérrez-Pastor, J., Nelson, C. H., Goldfinger, C. & Escutia, C. Sedimentology of seismo-turbidites off the Cascadia and northern California active tectonic continental margins, northwest Pacific Ocean. *Mar. Geol.* **336**, 99–119 (2013).
35. Van Daele, M. et al. A revised classification and terminology for stacked and amalgamated turbidites in environments dominated by (hemi)pelagic sedimentation. *Sediment. Geol.* **357**, 72–82 (2017).
36. Talling, P. J., Masson, D. G., Sumner, E. J. & Malgesini, G. Subaqueous sediment density flows: depositional processes and deposit types. *Sedimentology* **59**, 1937–2003 (2012).
37. Ho, V. L., Dorrell, R. M., Keevil, G. M., Burns, A. D. & McCaffrey, W. D. Pulse propagation in turbidity currents. *Sedimentology* **65**, 620–637 (2018).
38. Barnes, P. M. & Audru, J. C. Quaternary faulting in the offshore Flaxbourne and Wairarapa basins, southern Cook Strait, New Zealand. *N. Z. J. Geol. Geophys.* **42**, 349–367 (1999).
39. Ho, V. L., Dorrell, R. M., Keevil, G. M., Burns, A. D. & McCaffrey, W. D. Scaling analysis of multipulsed turbidity current evolution with application to turbidite interpretation. *J. Geophys. Res. Oceans* **123**, 3668–3684 (2018).
40. Ho, V. L. et al. Dynamics and deposition of sediment-bearing multi-pulsed flows and geological implication. *J. Sediment. Res.* **89**, 1127–1139 (2019).
41. Paull, C. K. et al. Origins of large crescent-shaped bedforms within the axial channel of Monterey Canyon, offshore California. *Geosphere* **6**, 755–774 (2010).
42. Adams, J. Paleoseismicity of the Cascadia subduction zone: evidence from turbidites off the Oregon–Washington Margin. *Tectonics* **9**, 569–583 (1990).
43. Downes, G. & Dowrick, D. *Atlas of isoseismal maps of New Zealand earthquakes—1843–2003* 2nd edn (revised) (GNS Science, 2014).
44. Pouderoux, H., Proust, J. N. & Lamarche, G. Submarine paleoseismology of the northern Hikurangi subduction margin of New Zealand as deduced from turbidite record since 16 ka. *Quat. Sci. Rev.* **84**, 116–131 (2014).
45. Clark, K. et al. Geological evidence for past large earthquakes and tsunamis along the Hikurangi subduction margin, New Zealand. *Mar. Geol.* **412**, 139–172 (2019).
46. Bradley, B. A. et al. Ground motion simulations of great earthquakes on the Alpine Fault: effect of hypocentre location and comparison with empirical modelling. *N. Z. J. Geol. Geophys.* **60**, 188–198 (2017).
47. Kearse, J., Kaneko, Y., Little, T. & Van Dissen, R. Curved slickenlines preserve direction of rupture propagation. *Geology* **47**, 838–842 (2019).
48. Moernaut, J. et al. Lacustrine turbidites produced by surficial slope sediment remobilization: a mechanism for continuous and sensitive turbidite paleoseismic records. *Mar. Geol.* **384**, 159–176 (2017).
49. Wartman, J., Seed, R. B. & Bray, J. D. Shaking table modeling of seismically induced deformations in slopes. *J. Geotech. Geoenviron. Eng.* **131**, 610–622 (2005).

Methods

Site selection and core sampling. Thirty-one cores from along 700 km of the HSM were retrieved using an Ocean Instruments MC800 multicorer, facilitating precision sampling of the sediment/water interface in sediment cores up to 70 cm in length. The corer was equipped with an ultrashort baseline acoustic beacon with positional accuracies on the sea floor of <10 m. This spatial precision allowed the majority of cores to be acquired from proximal locations slightly offset from the canyon thalweg but generally <10 vertical m from it (Supplementary Figs. 2–13). By locating core sites in this way, we minimize the potential influence of both erosive flows in the channel thalweg and variations in turbidity-current height on the presence/absence and sedimentary structures of turbidites[9,14,41,50]. Cores sited 30–40 m above the canyon thalweg (TAN1705 22, 25, and 27) avoid morphological and sedimentological features in the entrenched thalweg that were not conducive to coring, such as gravel deposits and/or scours (Supplementary Figs. 7, 8 and 11).

Cores were photographed and logged visually in the field and then analysed ashore using X-ray CT conducted on a General Electric BrightSpeed medical CT scanner set to 120 kV, 250 mA, pitch of 0.625 mm and a 100 cm² window. CT was processed in the software ImageJ to produce sagittal slice images and down-core density curves at 625 µm resolution using the relationship of Reilly et al.[51] for deriving bulk density from Hounsfield value/CT number. Cores were also line-scan imaged and logged visually. High-resolution grain-size analysis (~2.5 mm resolution) was conducted on the turbidites from selected cores using a Beckman Coulter LS 13 320 Multi-Wavelength Laser Diffraction Particle Size Analyser to establish the relationship between CT-derived bulk density and mean grain size. The geochemical composition of cores was characterized with micro-X-ray fluorescence core scanning using a COX analytical systems Itrax X-ray-fluorescence core scanner at a down-core resolution of 1 mm.

Geochronology. Radiometric dating of turbidite sediments using the short-lived radioisotope ^{234}Th, which has a half-life of 24 days, provided quantitative evidence for recent emplacement. Once sediment is isolated from seawater through deposition, excess ^{234}Th activity becomes undetectable within 5 half-lives (120 days) of deposition. Consequently, the presence of excess ^{234}Th in the turbidite and the sediments that immediately underlie it provides evidence for very recent deposition. Radionuclide measurements were made on sediment from core TAN1613 53 from the Hikurangi trough using gamma spectrometry at the Institute of Environmental Science and Research using a high-purity germanium detector. Excess ^{234}Th was determined by repeat measurements where the initial samples were measured within 3 half-lives of the earthquake (72 days). Supported ^{234}Th was determined by remeasuring each sample after 5 half-lives (120 days) had elapsed. The reported excess ^{234}Th activities have been decay corrected to the date of the earthquake. ^{210}Pb was measured by chemically separating its daughter product, ^{210}Po, and measuring its activity using alpha spectrometry. Activities for both radioisotopes are reported in Bq kg^{-1} and the uncertainties are based on the combined standard uncertainty multiplied by a coverage factor ($k=2$, providing a level of confidence of 95%).

The quantitative geochronology was used alongside CT, high-resolution imagery and geochemistry to develop qualitative indices of recent deposition from the TAN1613 53 core site. These indices include: (1) the presence of an oxic layer indicative of sedimentary material recently at the sediment–water interface located immediately underlying turbidites, (2) a lack of bioturbation in freshly deposited coseismic turbidites at core tops and (3) the presence of fresh biological remains in the turbidite and, where possible, pre- and post-earthquake coring[33]. Oxic layers were identified visually and using down-core measurements of Fe/Mn ratios, which provide indices for oxidation[52]. The degree of bioturbation was assessed using CT to compare trace fossil abundance within the inferred 2016 Kaikōura turbidite with that in the underlying pre-earthquake sea-floor sediment and in cores from other sites that lacked the 2016 Kaikōura turbidite at their core top. Repeat coring at selected sites assessed the degree of bioturbation that had occurred over the eight months between the earthquake and the last coring campaign. Once established, the qualitative indices of recent deposition were applied to identify the 2016 Kaikōura turbidite in the other cores from along the margin because their date of coring, eight months after the earthquake, precluded the use of ^{234}Th dating.

Ground-motion modelling. To simulate realistic Kaikōura earthquake waves, we used a source model of the earthquake developed previously[31] that fits local strong-motion and geodetic (Interferometric Synthetic Aperture Radar and Global Positioning System) data. We also followed the ground-motion simulation method as described in Holden et al.[29], in which synthetic ground motions were computed using open-source seismic wave propagation software SPECFEM3D (refs. [53,54]). This approach utilized 3D velocity and attenuation models for New Zealand[55] and topography and bathymetry of the region. The mesh spacing was 1 km on the Earth surface and became coarser with depth. The topography and bathymetry were from Shuttle Radar Topography Mission (SRTM) 30 and had a spatial resolution of 1–2 km. Numerical simulations were run on New Zealand's eScience Infrastructure supercomputing cluster and the seismic waves were numerically accurate down to 2 s (0.5 Hz). With the smallest shear-wave velocity of ~1 km s^{-1} assumed in the current model set up, the smallest length scale of geological features influencing resulting ground motions was of the order of several kilometres, which is comparable or smaller than the sizes of the canyon catchments that produced turbidity currents. Synthetic ground-motion time series, expressed as the magnitude of three-component particle velocities ($|\mathbf{v}|$), and corresponding PGV values were computed on a 4 km spaced grid covering onshore and offshore regions. We report PGV values rather than peak ground acceleration (PGA), which is usually used in marine palaeoseismic studies, because the PGV values have been validated against onshore strong-motion and high-rate Global Positioning System data along the entire Hikurangi margin[29].

The assumed 3D velocity model indicates the presence of the low-velocity sedimentary wedge of the outer forearc (Supplementary Fig. 21), although the resolution of the tomographic model offshore is relatively low. The presence of such a low-velocity zone amplifies the resulting ground motions via basin–directivity coupling[30], which may enhance the triggering of submarine landslides. To assess the effect of the uncertainty in the offshore velocity model on the simulated ground motions at turbidite sources/underwater canyons, we computed synthetic ground motions using a one-dimensional (1D), layered velocity model (Supplementary Fig. 18). The 1D velocity model was derived from the spatial average of P- and S-wave seismic velocities (V_P and V_S, respectively), densities and anelastic attenuations (Q_P and Q_S) at different depth slices in the 3D velocity model.

Including the assumed 3D shear-wave velocity model in the ground-motion simulation resulted in a band of high PGV extending from the northern tip of the Kaikōura fault rupture, ~300 km along the upper continental slope of the outer forearc. In this model PGVs are elevated above those produced by the 1D model in the area of turbidity-current triggering by a factor of two on average (Supplementary Fig. 18). Both models produced consistent threshold relationships between triggering and no triggering of turbidity currents but the threshold PGV for the 3D simulation ranges between 16 and 25 cm s^{-1} compared with between just ~8 and 10 cm s^{-1} for the 1D equivalent. We adopted the 3D simulation as the preferred model because the PGVs produced by it showed better fit to the observed station data than those from the 1D model (Supplementary Fig. 17). PGVs and velocity time histories were extracted from the centroid of each canyon catchment. For slope basins, the slopes bounding the basin nearest the centroid were used because the very low gradient floor of these basins was deemed unlikely to be a source for turbidity currents. The PGV for the Kaikōura canyon was derived from a location within the distribution of coseismic landsliding on the canyon rim mapped by Mountjoy et al.[33].

Comparison between amplitude peaks in ground-velocity time histories for each catchment centroid and the number of grain-size pulses in the associated turbidite was conducted using a simple pass/fail test. As the specific ground-velocity triggering threshold for each catchment remains unknown, it is not possible to directly compare the number of grain-size pulses and velocity amplitude peaks above that threshold. Taking into account the range of potential triggering thresholds, turbidite structure was deemed consistent with the ground-velocity time history of the earthquake when the number of velocity peaks with amplitudes within the regional triggering-threshold range (16–25 cm s^{-1}) was greater than or equal to the number of grain-size pulses in the turbidite. Conversely, turbidite structure and the ground-motion time histories were deemed inconsistent when either: (1) the number of grain-size pulses exceeded the number of velocity peaks that reach the triggering-threshold range or (2) fewer grain-size pulses were observed than the number of velocity peaks exceeding the upper bound of the triggering-threshold range (that is, 25 cm s^{-1}).

Morphometric analysis of canyons. Morphometric analysis of the distributary canyons was undertaken in the software package ArcMap v.10.8 on a 100 m Multibeam Echosounder (MBES)-derived bathymetric grid. The average distance from turbidity-current source areas to the core site, upstream thalweg length and gradient, and the number of upstream major confluences were determined using the Hydrology toolset. Contributing catchment areas were manually digitized and used to produce a flow-accumulation raster that guided channel definition. Thalweg length and gradient were derived from the bathymetric grid by interpolating surface measurements along the main thalweg polyline. Turbidity current source areas were determined using a slope threshold of 5.5°, which is the slope threshold for submarine gullying in the southern HSM[56]. For each canyon catchment, downslope flow direction from the source area pixels to the core site was constrained using the eight-direction (D8) flow raster to create flow paths between adjacent cells.

Data availability

Core sedimentological (bulk density, grain size and geochemistry), geochronological and modelled ground-motion datasets generated during and/or analysed during the current study are available in the Figshare repository: https://doi.org/10.6084/m9.figshare.13359101.v1. The regional bathymetry (250 m grid) data that support the findings of this study can be downloaded from the New Zealand Bathymetry database website: https://niwa.co.nz/our-science/oceans/bathymetry. Where available, high-resolution bathymetry (25 m grid) data used in the current study are from NIWA's data holdings and were used under a data-sharing agreement with NIWA for the current study. Data are however available for research purposes from the authors upon reasonable request and with the permission of NIWA. Source data are provided with this paper.

Code availability

The open-source software SPECFEM3D used in our ground-motion simulations is available from the Computational Infrastructure for Geodynamics at: https://geodynamics.org/cig/software/specfem3d/.

References

50. Covault, J., Sylvester, Z., Hubbard, S., Jobe, Z. & Sech, R. The stratigraphic record of submarine-channel evolution. *Sediment. Rec.* **14**, 4–11 (2016).
51. Reilly, B. T., Stoner, J. S. & Wiest, J. SedCT: MATLAB™ tools for standardized and quantitative processing of sediment core computed tomography (CT) data collected using a medical CT scanner. *Geochem. Geophys. Geosyst.* **18**, 3231–3240 (2017); https://doi.org/10.1002/2017GC006884
52. Rothwell, R. G. & Croudace, I. W. in *Micro-XRF Studies of Sediment Cores: Applications of a Non-destructive Tool for the Environmental Sciences* (eds Croudace, I. W. & Rothwell, R. G.) 25–102 (Springer, 2015).
53. Komatitsch, D. & Tromp, J. Introduction to the spectral element method for three-dimensional seismic wave propagation. *Geophys. J. Int.* **139**, 806–822 (1999).
54. Komatitsch, D. & Vilotte, J.-P. The spectral element method: an efficient tool to simulate the seismic response of 2D and 3D geological structures. *Bull. Seismol. Soc. Am.* **88**, 368–392 (1998).
55. Eberhart-Phillips, D. & Bannister, S. 3-D imaging of the northern Hikurangi subduction zone, New Zealand: variations in subducted sediment, slab fluids and slow slip. *Geophys. J. Int.* **201**, 838–855 (2015).
56. Micallef, A. & Mountjoy, J. J. A topographic signature of a hydrodynamic origin for submarine gullies. *Geology* **39**, 115–118 (2011).

Acknowledgements

Funding for core analysis was provided by an Earthquake Commission (EQC) biennial research grant (No. 18/756) awarded to J.D.H., A.R.O. and S.D.N. and a Marsden grant (MFP-19-NIW-027) awarded to J.D.H. and A.R.O. Voyages in 2016 and 2017 were funded by Ministry of Business, Innovation and Employment (MBIE) Tangaroa Reference Group and the MBIE Endeavour programme 'Diagnosing peril posed by the Hikurangi subduction zone' (CONT-46722-CRFRP-GNS). National Institute of Water and Atmospheric Research (NIWA) scientists were cofunded by a MBIE Strategic Science Investment Fund in the Physical Resources programme in NIWA's Coasts and Oceans Centre. Y.K. was funded by a Rutherford Foundation Discovery Fellowship. Simulations of seismic wave propagation were run on the New Zealand eScience Infrastructure high-performance computing facilities. We thank J. Wartman for informative discussions on slope failure mechanisms.

Author contributions

J.D.H. designed the study with input from A.R.O. and Y.K. P.M.B., J.D.H. and J.J.M. identified core sites. J.D.H., A.R.O., S.D.N. and P.M.B. undertook the field sampling. J.D.H., A.R.O., L.J.S., H.C.B., S.D.N. and M.N.C. generated and interpreted the core sedimentological and geochemical data. Y.K. and C.H. conducted the ground-motion modelling. K.J. conducted the morphometric analysis. J.D.H. and A.R.O. wrote the paper with input from all co-authors.

Competing interests

The authors declare no competing interests.

Additional information

Supplementary information The online version contains supplementary material available at https://doi.org/10.1038/s41561-021-00692-6.

Correspondence and requests for materials should be addressed to J.D.H.

Peer review information Primary handling editor: Stefan Lachowycz. *Nature Geoscience* thanks Karim Tarbali, Peter Talling and Ken Ikehara for their contribution to the peer review of this work

Reprints and permissions information is available at www.nature.com/reprints.

nature portfolio

https://doi.org/10.1038/s41561-021-00692-6

Supplementary information

Calibrating the marine turbidite palaeoseismometer using the 2016 Kaikōura earthquake

In the format provided by the authors and unedited

Supplementary Information

Calibrating the marine turbidite paleoseismometer using the 2016 Kaikōura earthquake

Jamie D. Howarth, Alan R. Orpin, Yoshihiro Kaneko, Lorna J. Strachan, Scott D. Nodder, Joshu J. Mountjoy, Philip M. Barnes, Helen C. Bostock, Caroline Holden, Katie Jones and M. Namik Cağatay

Table of content:

Potential for aftershock triggering of turbidity currents

Analysis of ground motions produced by aftershocks with M>5.8 demonstrates that they were not capable of generating sufficient strong ground motions in the canyons to trigger turbidity currents (Supplementary Figure 1).

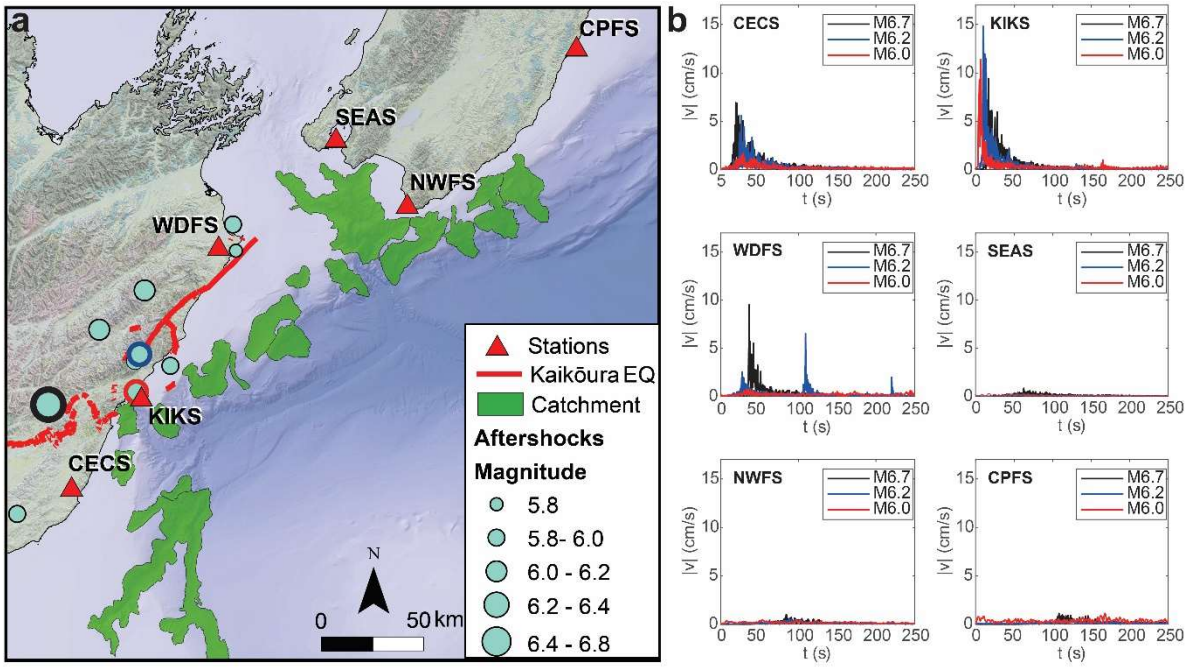

Supplementary Figure 1: The location of aftershocks with magnitudes M>5.8 and observed velocity-time histories for representative examples. a, Aftershock location with respect to the mainshock rupture and the canyons investigated in this study (aftershock locations from Geonet (https://quakesearch.geonet.org.nz/) or Meng et al.[1] if relocated). All ten aftershocks with M>5.8 are located a minimum of 6.5 km from the nearest canyon heads. The closest aftershock to the canyon heads has a magnitude of M5.8. Aftershock 2016p858021 (dot outlined in red) has a magnitude of M6.0, is located at a depth of 5.6 km and just 2.8 km from the KIKS strong ground motion station[1]. The distance between this aftershock and KIKS is less than the minimum distance to the canyons. Consequently, the aftershock provides a suitable test of whether aftershocks are capable of generating ground motions equivalent to the minimum turbidite emplacement threshold (>16 $cm.s^{-1}$) at the canyon locations. **b,** Velocity-time histories for representative M>5.8 aftershocks at ground motion stations in the north eastern South Island and the south eastern North Island (locations marked by dots with coloured outlines in a). Despite the proximity of the M6.0 aftershock to the KIKS station peak ground velocity of long period motions do not exceed 11 cm s^{-1}. Furthermore, none of the other representative aftershocks produced ground motions at any of the stations in excess of 15 cm s^{-1}. As all these aftershocks were located landward of the four coastal stations it is reasonable to infer that no aftershocks generated long period motions sufficient to trigger turbidity currents in the canyons.

Core site locations

Supplementary table 1 and figures 2 through 13 show the bathymetric setting of the core sites that contain turbidites deposited by the 2016 Kaikōura earthquakes and the canyons with no turbidite at the surface/water interface at the southern and northern extents of triggering.

Supplementary table 1: Summary of core site and canyon morphometric parameters.

Core site	Height (m) above centre of the channel	Average distance to source areas (km)	Distributary catchment area (km^2)	Confluences	Turbidite signature (#pulses)	Ground velocity peaks vs pulses
TAN1705-38	10				No turbidite	Pass
TAN1705-37	6				No turbidite	Pass
TAN1705-36	4	10	160	1	Single pulse	Pass
TAN1705-33	9	14	353	1	Single pulse	Pass
TAN1705-32	4	11	50	1	Single pulse	Pass
TAN1705-31	2	10	250	0	Multipulse (2)	Pass
TAN1705-26	6	15	190	0	Multipulse (3)	Pass
TAN1705-27	30	50	1330	3	Multipulse (3-5)	Pass
TAN1705-25	32	25	480	2	Multipulse (3)	Pass
TAN1705-24	2	12.5	210	0	Multipulse (3)	Fail
TAN1705-23	8	20	410	0	Equivocal multi-pulse (2)	Pass
TAN1705-22	40				No turbidite	Pass

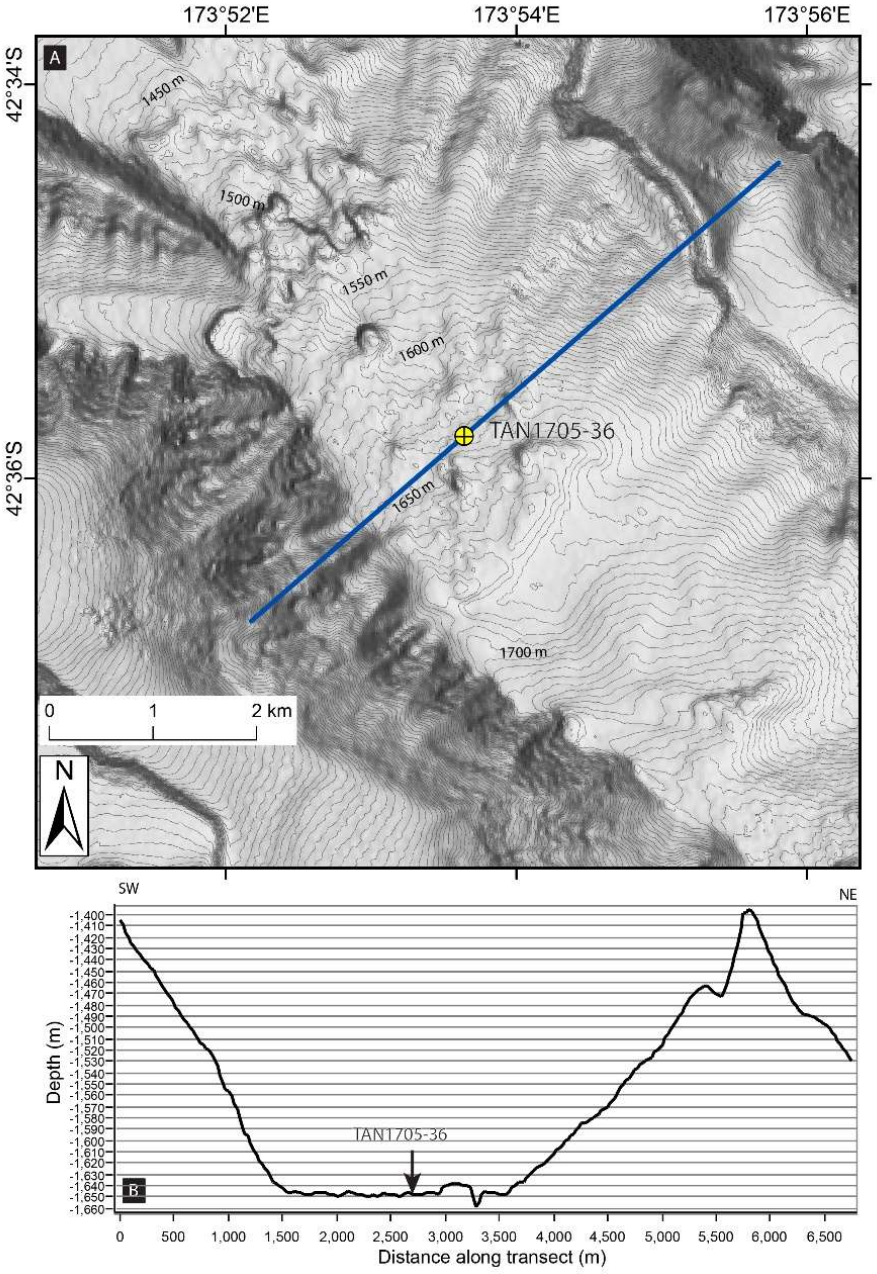

Supplementary Figure 2. Bathymetric setting of core site TAN1705-36.

Lat. -42.5964, Long. 173.8940. Water depth 1647 m.

Presence of 2016 M_w 7.8 Kaikōura earthquake turbidite: Yes.

a, Bathymetric map derived from SIMRAD Kongsberg EM302 multibeam data gridded to 25 m, showing bathymetric contours at 5 m intervals draped over a multi-directional hillshade with vertical exaggeration of 2. Multicore TAN1705-36 is located on the middle continental slope off northeastern South Island, in the Kowhai Sea-valleys. The core is positioned to within an accuracy of 10 m, using an ultra-short baseline (USBL) underwater acoustic positioning system on R.V. *Tangaroa*. The site lies within a channel that traverses normal to the slope, and is located approximately 2 km below the junction of three major tributaries. The channel floor in the vicinity of the core site is irregular, and about 2 km wide. **b,** Bathymetric cross-section through the core site showing the site is located in the centre of the channel, and lies 4 m above the maximum channel depth.

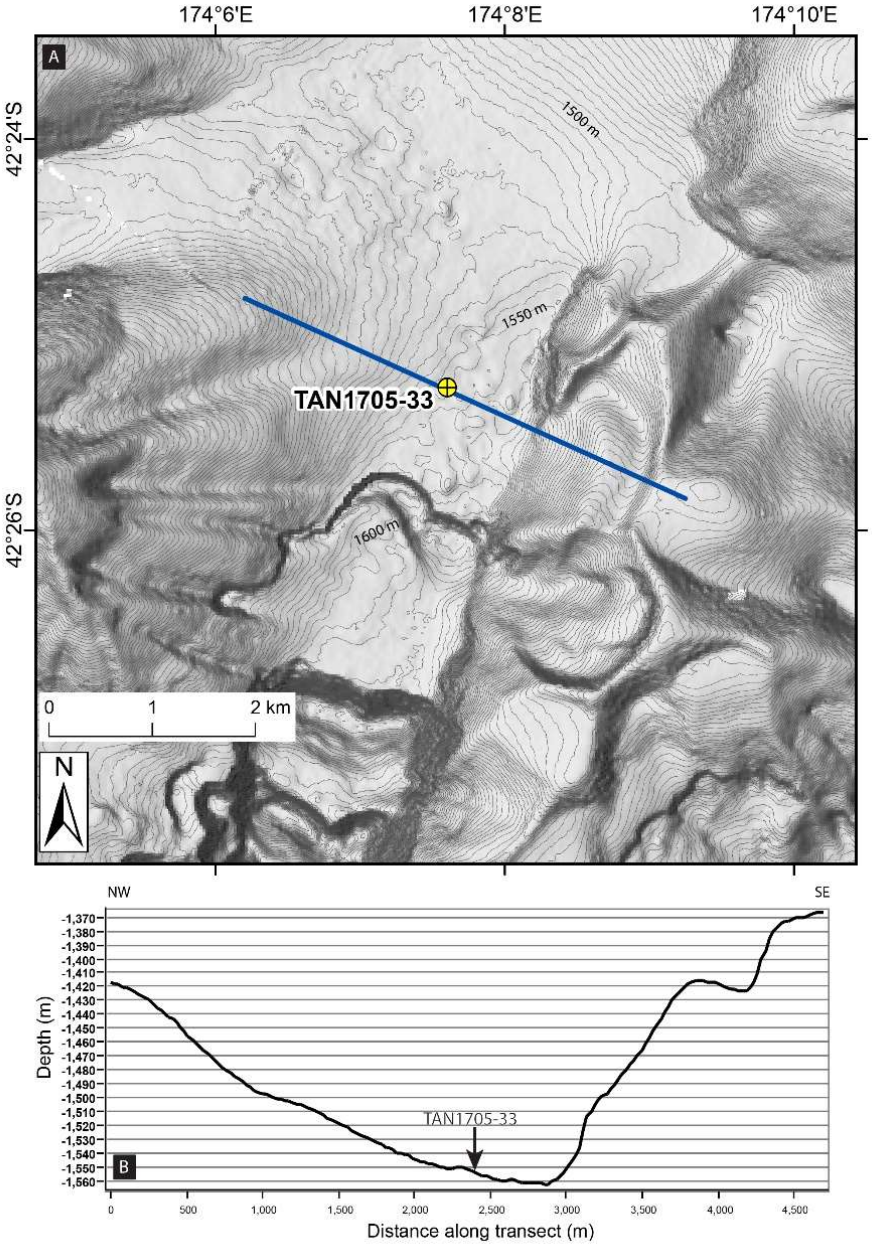

Supplementary Figure 3. Bathymetric setting of core site TAN1705-33

Lat. --42.4212, Long. 174.1267. Water depth 1541 m.

Presence of 2016 M_w 7.8 Kaikōura earthquake turbidite: Yes.

a, Bathymetric map derived from SIMRAD Kongsberg EM302 multibeam data gridded to 25 m, showing bathymetric contours at 5 m intervals draped over a multi-directional hillshade with vertical exaggeration of 2. Multicore TAN1705-33 is located on the middle continental slope off northeastern South Island, at the northern end of the Kowhai Sea-valleys. The core is positioned to within an accuracy of 10 m, using an ultra-short baseline (USBL) underwater acoustic positioning system on R.V. *Tangaroa*. The site lies within a 700-800 m wide channel approximately 2 km below the junction of tributaries, and 1 km above prominent steps in the channel morphology. **b,** Bathymetric cross-section through the core site showing the site is located in the western side of the channel, about 9 m above the maximum channel depth along the eastern boundary.

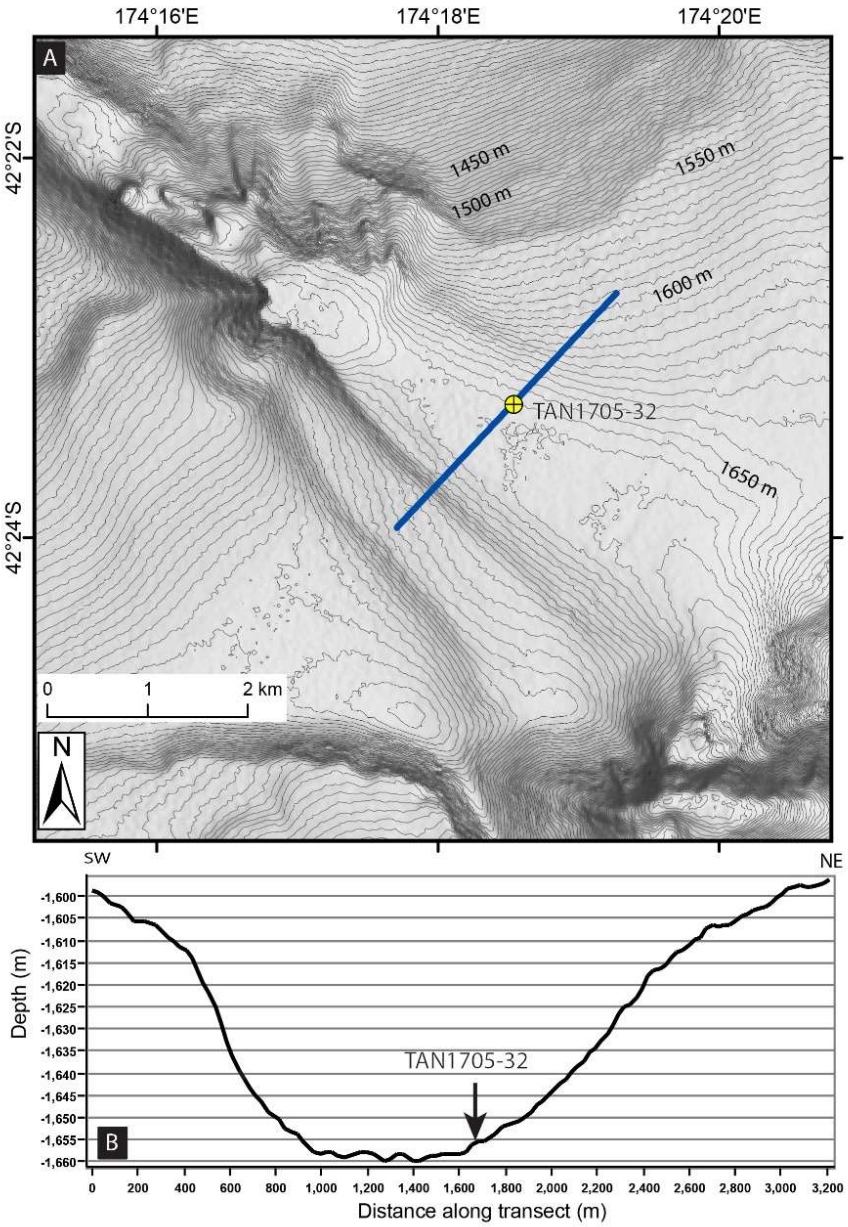

Supplementary Figure 4. Bathymetric setting of core site TAN1705-32

Lat. -42.3883, Long. 174.3090. Water depth 1655 m.

Presence of 2016 M_w 7.8 Kaikōura earthquake turbidite: Yes.

a, Bathymetric map derived from SIMRAD Kongsberg EM302 multibeam data gridded to 25 m, showing bathymetric contours at 5 m intervals draped over a multi-directional hillshade with vertical exaggeration of 2. Multicore TAN1705-32 is located on the middle continental slope off northeastern South Island, in an un-named channel NE of the Kowhai Sea-valleys. The core is positioned to within an accuracy of 10 m, using an ultra-short baseline (USBL) underwater acoustic positioning system on R.V. *Tangaroa*. The site lies within a 600-800 m wide channel that traverses normal to the slope, and is located approximately 2 km below a prominent break in slope. The break in slope is characterized by an elongate basin that separates an upslope, irregular section of the channel, from a smooth section crossing an inclined terrace. **b,** Bathymetric cross-section through the core site showing the site is located on the northern side of a channel, and lies 4 m above the maximum channel depth.

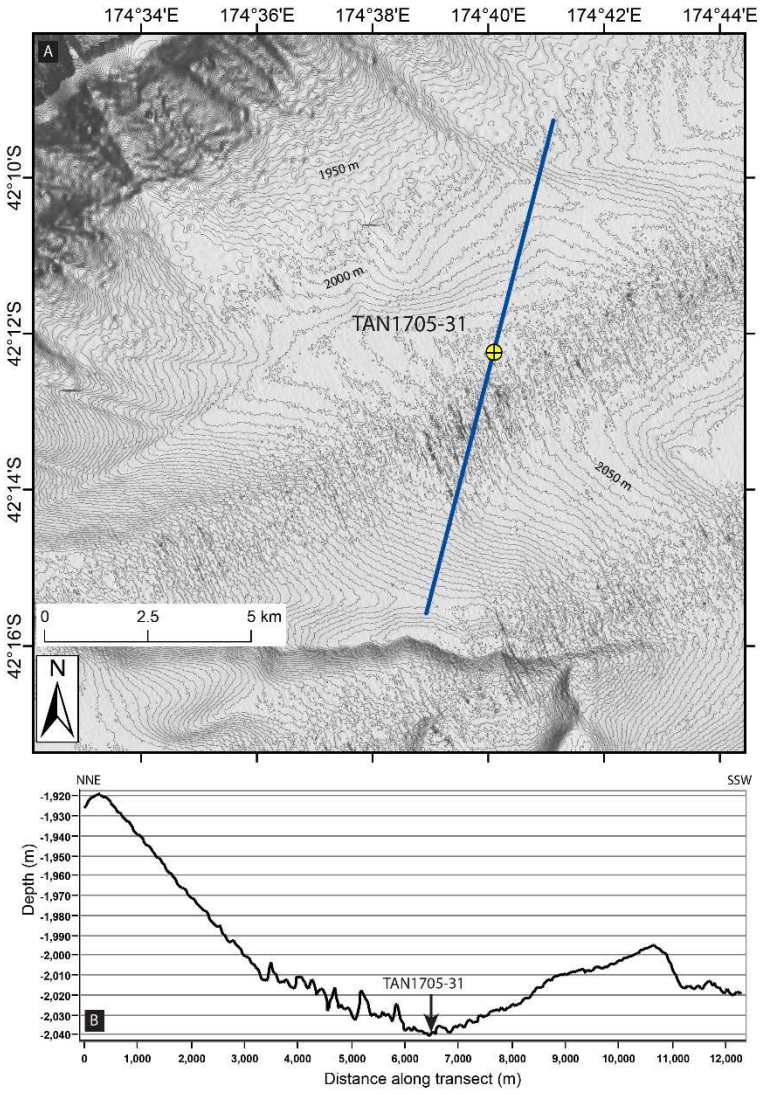

Supplementary Figure 5. Bathymetric setting of core site TAN1705-31

Lat. -42.2040, Long. 174.6683. Water depth 2039 m.

Presence of 2016 M_w 7.8 Kaikōura earthquake turbidite: Yes.

a, Bathymetric map derived from SIMRAD Kongsberg EM302 multibeam data gridded to 25 m, showing bathymetric contours at 5 m intervals draped over a multi-directional hillshade with vertical exaggeration of 2. Multicore TAN1705-31 is located on the middle continental slope off northeastern South Island. The core is positioned to within an accuracy of 10 m, using an ultra-short baseline (USBL) underwater acoustic positioning system on R.V. *Tangaroa*. The site lies within a broad un-named trough oriented oblique to the continental slope, and about 7-8 km below a prominent break in slope. **b,** Bathymetric cross-section through the core site showing the site is located in the centre of the trough, and lies 2 m above the maximum depth on the section.

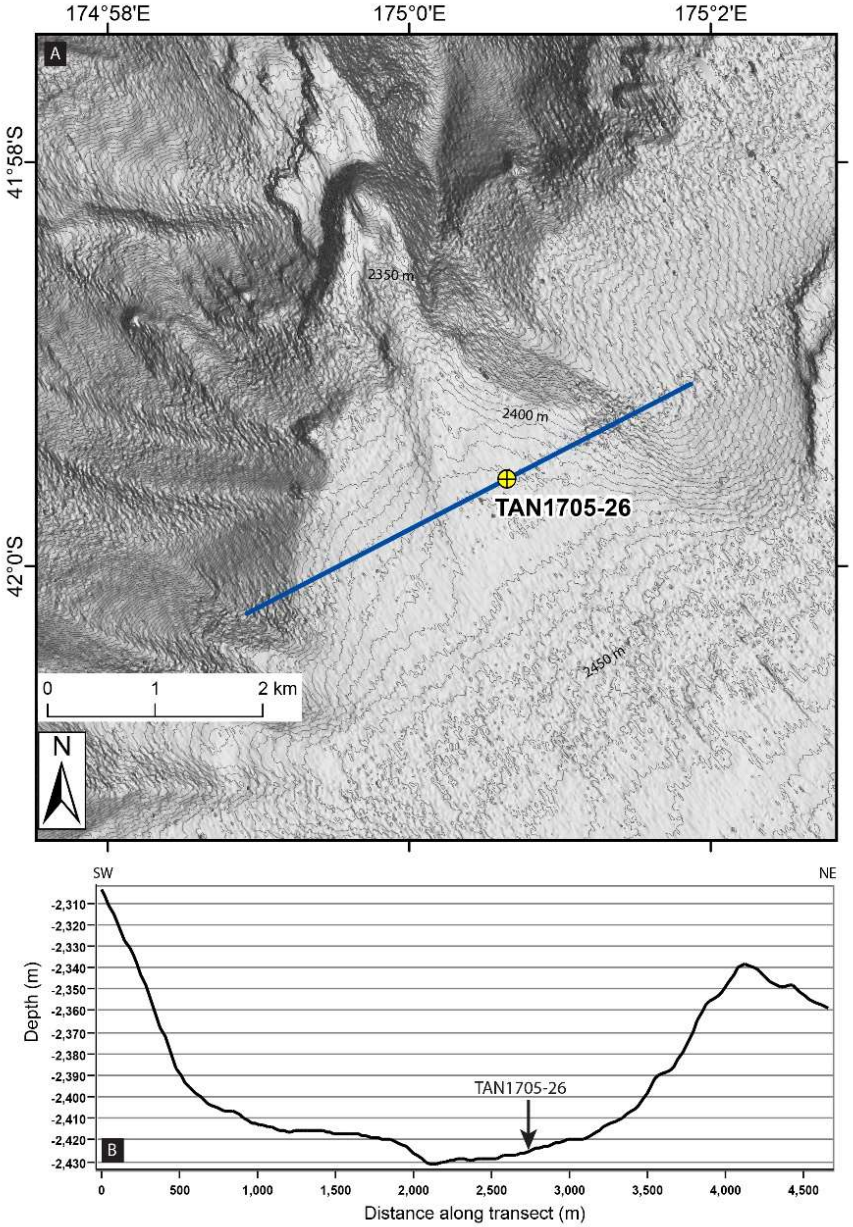

Supplementary Figure 6. Bathymetric setting of core site TAN1705-26

Lat. -41.9928, Long. 175.0108. Water depth 2423 m.

Presence of 2016 M_w 7.8 Kaikōura earthquake turbidite: Yes.

a, Bathymetric map derived from SIMRAD Kongsberg EM302 multibeam data gridded to 25 m, showing bathymetric contours at 5 m intervals draped over a multi-directional hillshade with vertical exaggeration of 2. Multicore TAN1705-26 is located on the middle continental slope off northeastern South Island. The core is positioned to within an accuracy of 10 m, using an ultra-short baseline (USBL) underwater acoustic positioning system on R.V. *Tangaroa*. The site lies at the mouth of a channel that traverses normal to the continental slope, and in the vicinity of a prominent break in the regional slope. The channel is about 1 km wide on the relatively steep slope above the site, widening to about 2 km at the site location. **b,** Bathymetric cross-section through the core site showing the site is located north of the channel centre, and lies 6 m above the maximum channel depth.

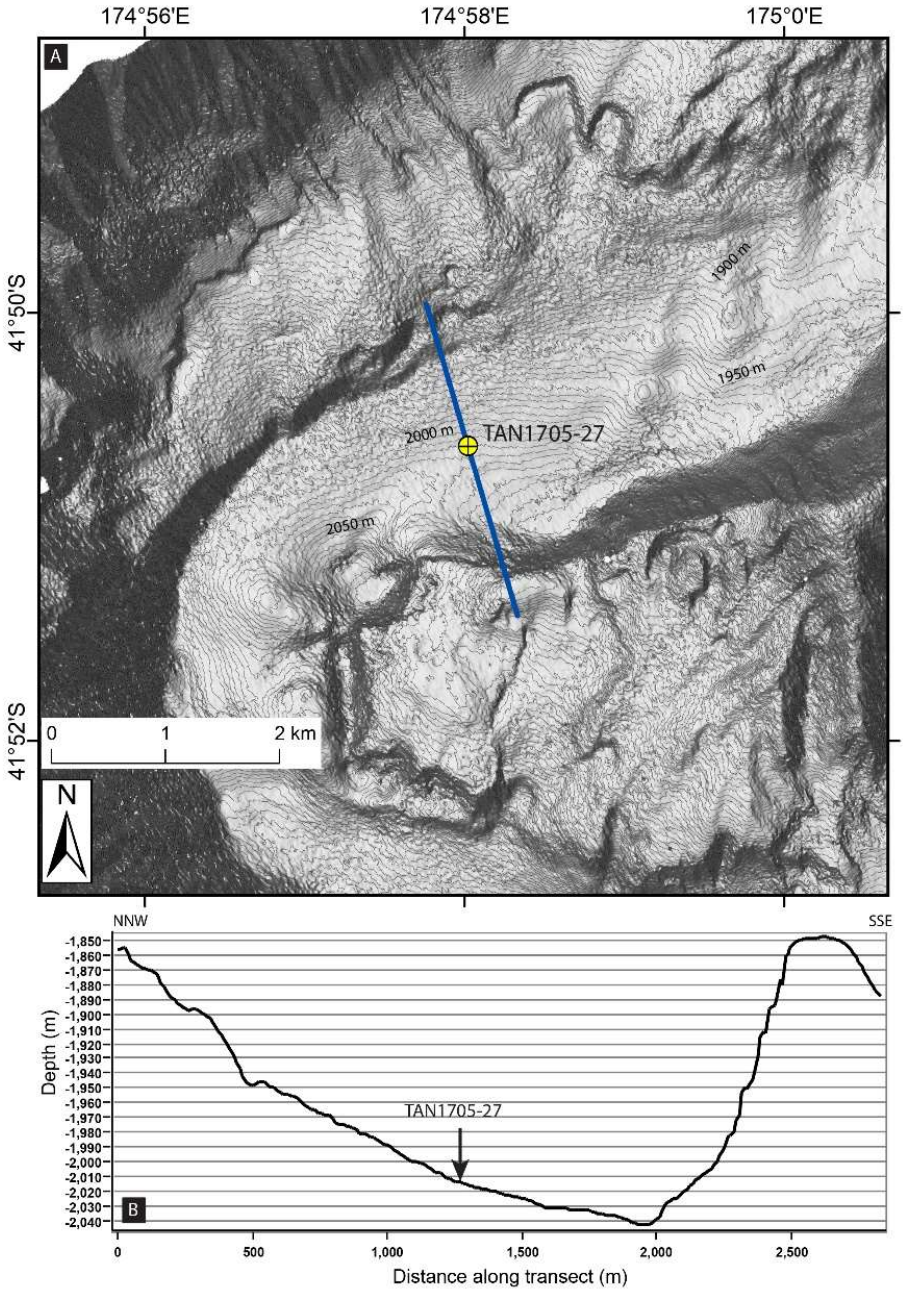

Supplementary Figure 7. Bathymetric setting of core site TAN1705-27

Lat. -41.8437, Long. 174.9670. Water depth 2015 m.

Presence of 2016 M_w 7.8 Kaikōura earthquake turbidite: Yes.

a, Bathymetric map derived from SIMRAD Kongsberg EM302 multibeam data gridded to 25 m, showing bathymetric contours at 5 m intervals draped over a multi-directional hillshade with vertical exaggeration of 2. Multicore TAN1705-27 is located in the lower, sinuous reaches of Cook Strait Canyon. The core is positioned to within an accuracy of 10 m, using an ultra-short baseline (USBL) underwater acoustic positioning system on R.V. *Tangaroa*. The site was positioned on a relatively smooth seafloor, upslope from depressions localized along the southern channel floor. **b,** Bathymetric cross-section showing the site is located in the centre of the 1 km-wide channel floor, and lies 30 m above the maximum channel depth along the southern boundary.

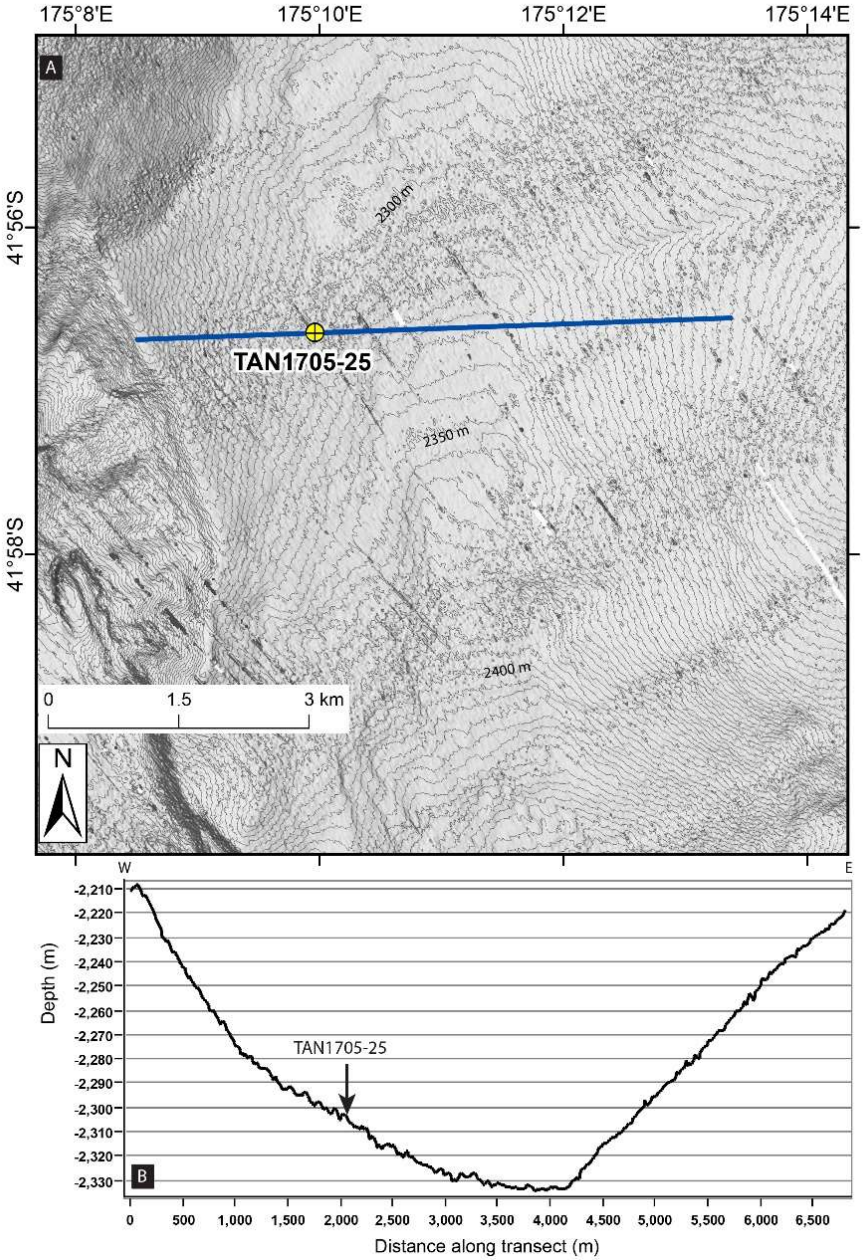

Supplementary Figure 8. Bathymetric setting of core site TAN1705-25

Lat. -41.9441, Long. 175.1660. Water depth 2304 m.

Presence of 2016 M_w 7.8 Kaikōura earthquake turbidite: Yes.

a, Bathymetric map derived from SIMRAD Kongsberg EM302 multibeam data gridded to 25 m, showing bathymetric contours at 5 m intervals draped over a multi-directional hillshade with vertical exaggeration of 2. Multicore TAN1705-25 is located on the lower continental slope off southeastern North Island, within the lower reaches of Opouawe Canyon. The core is positioned to within an accuracy of 10 m, using an ultra-short baseline (USBL) underwater acoustic positioning system on R.V. *Tangaroa*. The site was positioned on the edge of the channel to avoid gravelly substrates associated with strong acoustic backscatter. **b,** Bathymetric cross-section through the core site showing the site located on the southern side of the channel, and 32 m above the maximum channel depth.

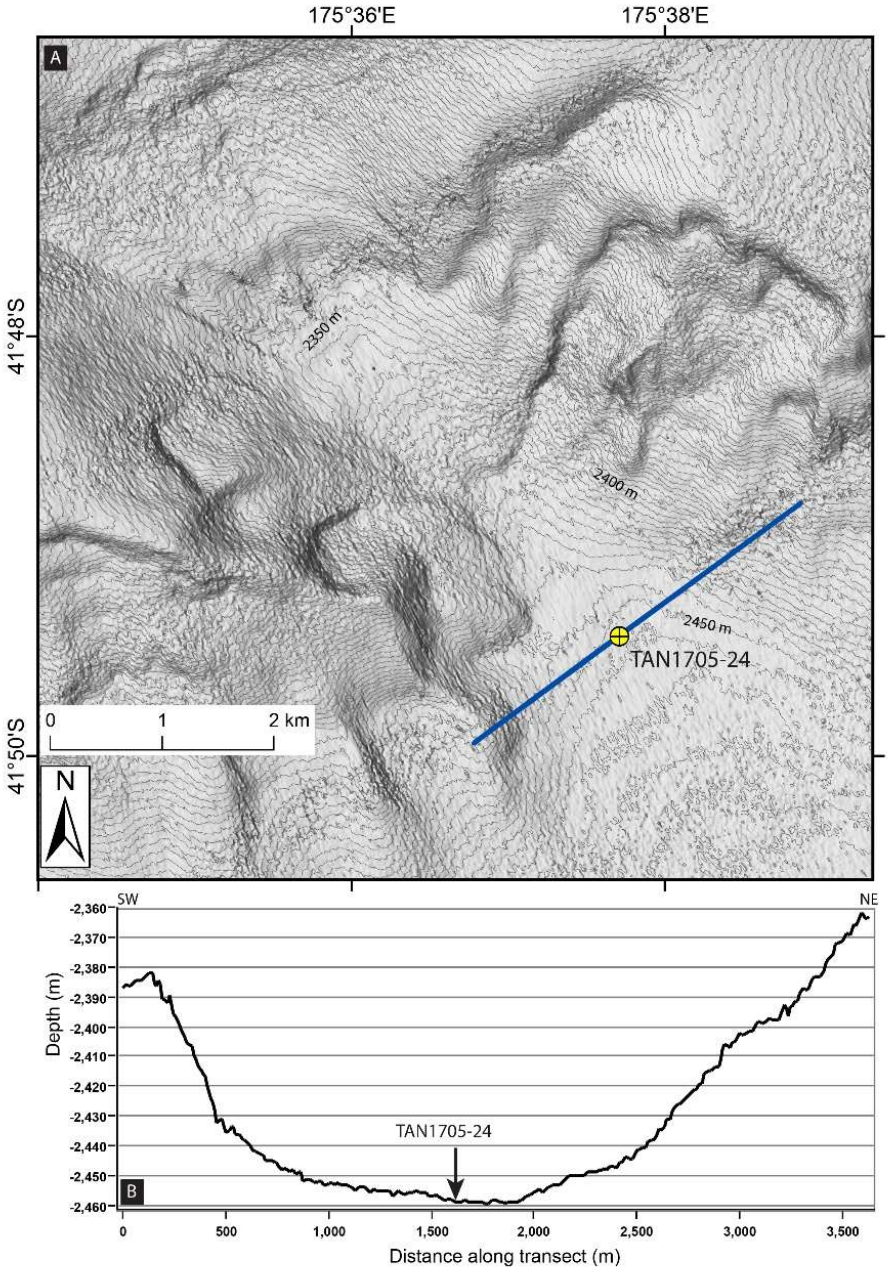

Supplementary Figure 9. Bathymetric setting of core site TAN1705-24

Lat. -41.8238 Long. 175.6285. Water depth 2459 m.

Presence of 2016 M_w 7.8 Kaikōura earthquake turbidite: Yes.

a, Bathymetric map derived from SIMRAD Kongsberg EM302 multibeam data gridded to 25 m, showing bathymetric contours at 5 m intervals draped over a multi-directional hillshade with vertical exaggeration of 2. Multicore TAN1705-24 is located on the lower continental slope off southeastern North Island, at the mouth of un-named channel system. The core is positioned to within an accuracy of 10 m, using an ultra-short baseline (USBL) underwater acoustic positioning system on R.V. *Tangaroa*. **b,** Bathymetric cross-section showing the site is located in the centre of the channel floor, which exceeds 1 km in width, and 2 m above the maximum channel depth.

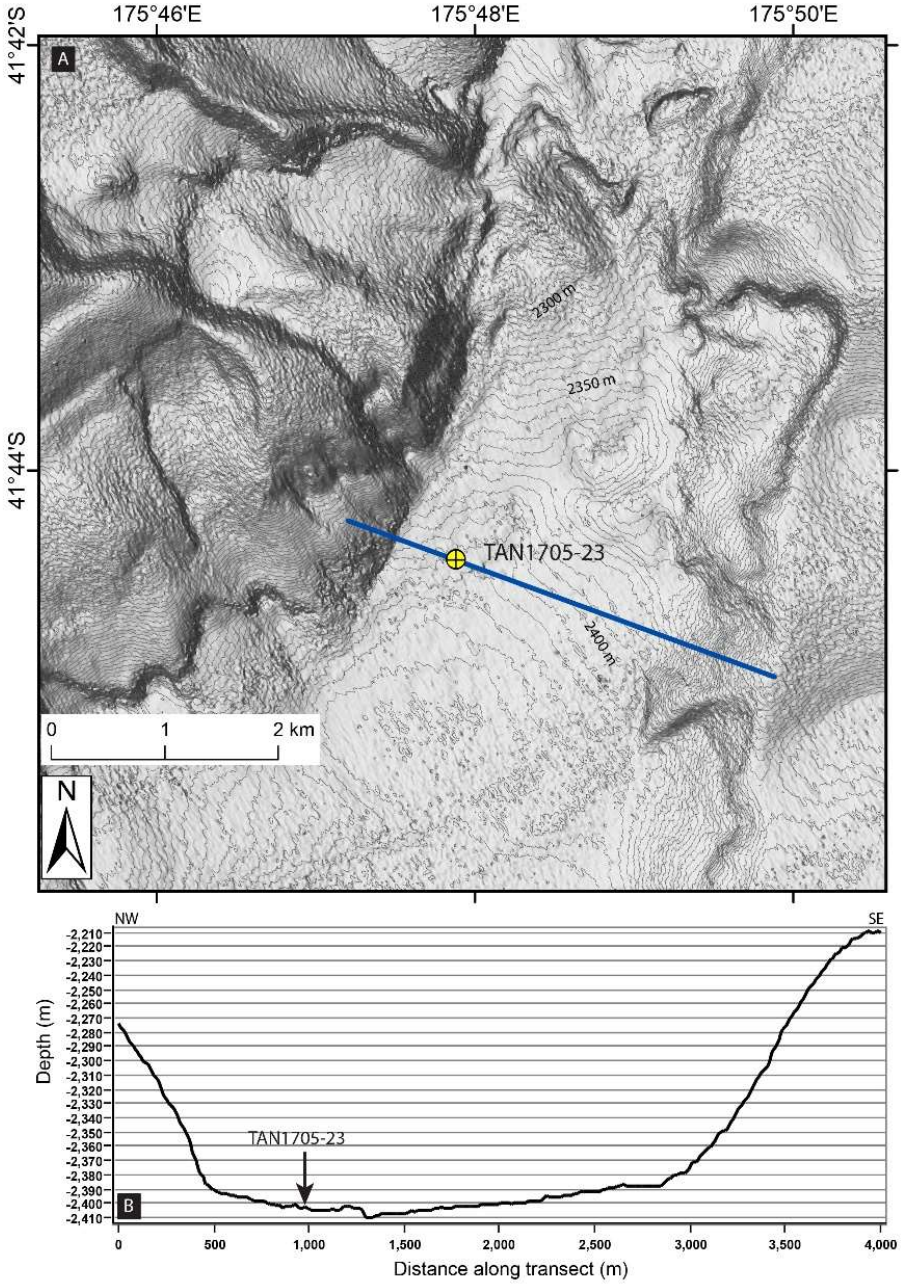

Supplementary Figure 10. Bathymetric setting of core site TAN1705-23

Lat. -41.7403, Long. 175.7977. Water depth 2403 m.

Presence of 2016 M_w 7.8 Kaikōura earthquake turbidite: Yes.

a, Bathymetric map derived from SIMRAD Kongsberg EM302 multibeam data gridded to 25 m, showing bathymetric contours at 5 m intervals draped over a multi-directional hillshade with vertical exaggeration of 2. Multicore TAN1705-23 is located on the lower continental slope off southeastern North Island, in the lower reaches of Pāhaoa Canyon. The core is positioned to within an accuracy of 10 m, using an ultra-short baseline (USBL) underwater acoustic positioning system on R.V. *Tangaroa*. The core is located on the southern side of the canyon floor, which is about 2 km wide in the vicinity of the site. **b,** Bathymetric cross-section showing the site is located 8 m above the maximum depth in the centre of the channel.

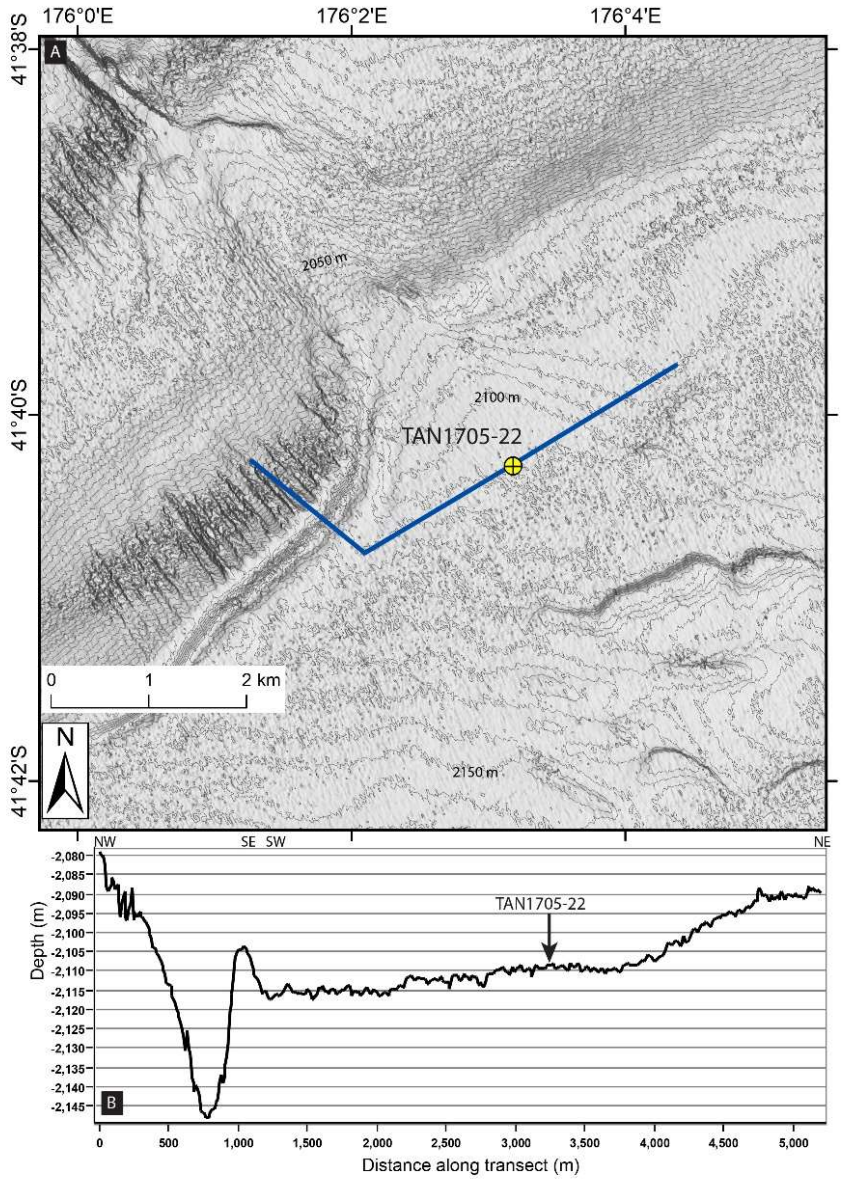

Supplementary Figure 11. Bathymetric setting of core site TAN1705-22

Lat. -41.6713, Long. 176.0530. Water depth 2108 m.

Presence of 2016 M_w 7.8 Kaikōura earthquake turbidite: No.

a, Bathymetric map derived from SIMRAD Kongsberg EM302 multibeam data gridded to 25 m, showing bathymetric contours at 5 m intervals draped over a multi-directional hillshade with vertical exaggeration of 2. Multicore TAN1705-22 is located on the lower continental slope off southeastern North Island, at the mouth of Honeycomb Canyon. The core is positioned to within an accuracy of 10 m, using an ultra-short baseline (USBL) underwater acoustic positioning system on R.V. *Tangaroa*. The site lies at a regional break in slope where turbidity currents enter the Glenhu Trough before flowing SW. The site is positioned between the break in slope upstream, and a series of radiating scour holes in the trough basin floor, downstream. A narrow gully is evident west of the core site at the base of the gullied slope. **b,** Bathymetric cross-section showing the site is located about 40 m above the axis of the narrow gully west of the site.

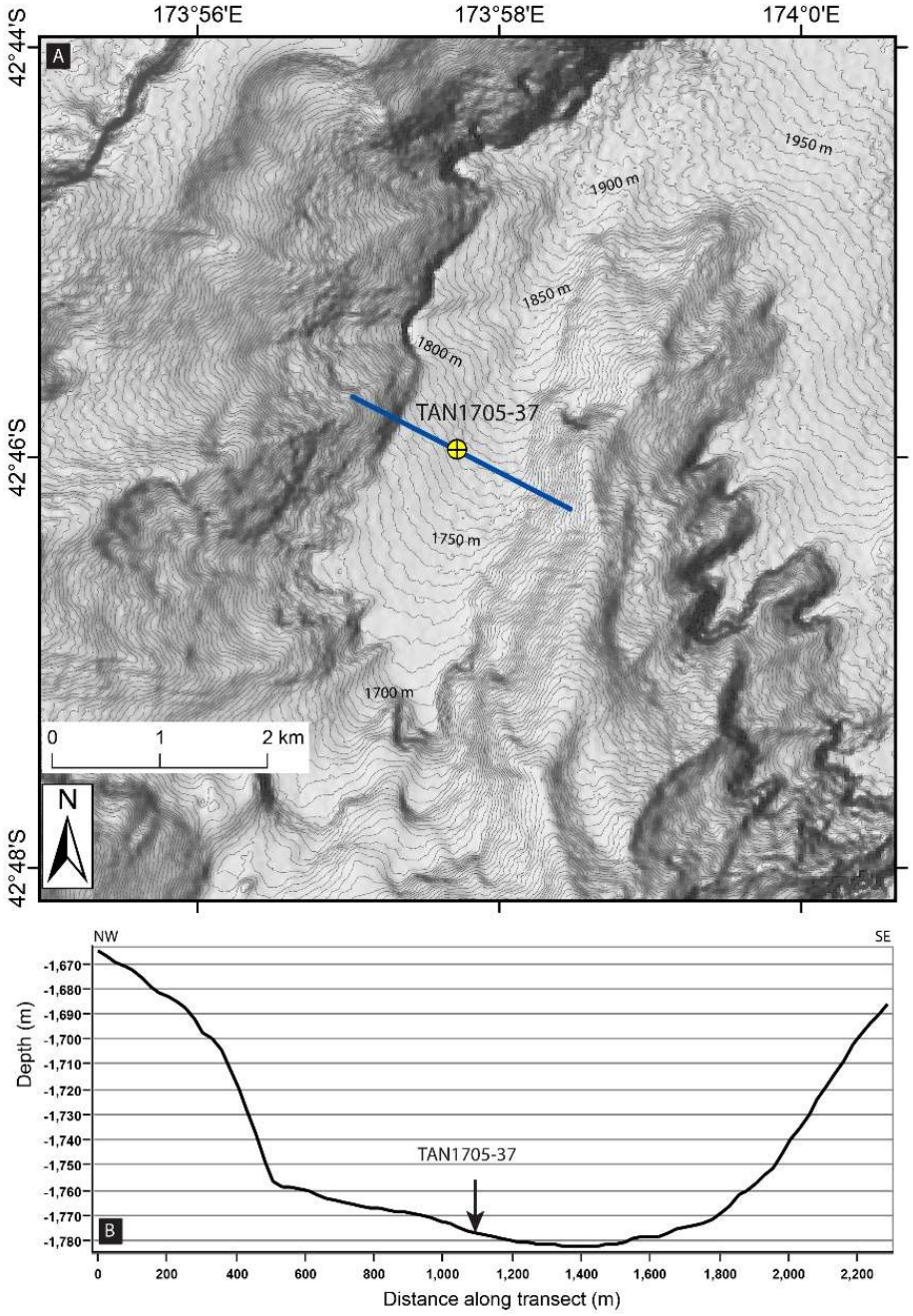

Supplementary Figure 12. Bathymetric setting of core site TAN1705-37

Lat. -42.7660, Long. 173.9620. Water depth 1776 m.

Presence of 2016 M_w 7.8 Kaikōura earthquake turbidite: No.

a, Bathymetric map derived from SIMRAD Kongsberg EM302 multibeam data gridded to 25 m, showing bathymetric contours at 5 m intervals draped over a multi-directional hillshade with vertical exaggeration of 2. Multicore TAN1705-37 is located on the continental slope off northeastern South Island, in the lower reaches of Hurunui Canyon. The core is positioned to within an accuracy of 10 m, using an ultra-short baseline (USBL) underwater acoustic positioning system on R.V. *Tangaroa*. The site lies within a 1.3 km-wide section of the channel, about 3-4 km above the confluence with Pegasus Canyon. **b,** Bathymetric cross-section showing the site is located in the centre of the channel, 6 m above the maximum channel depth.

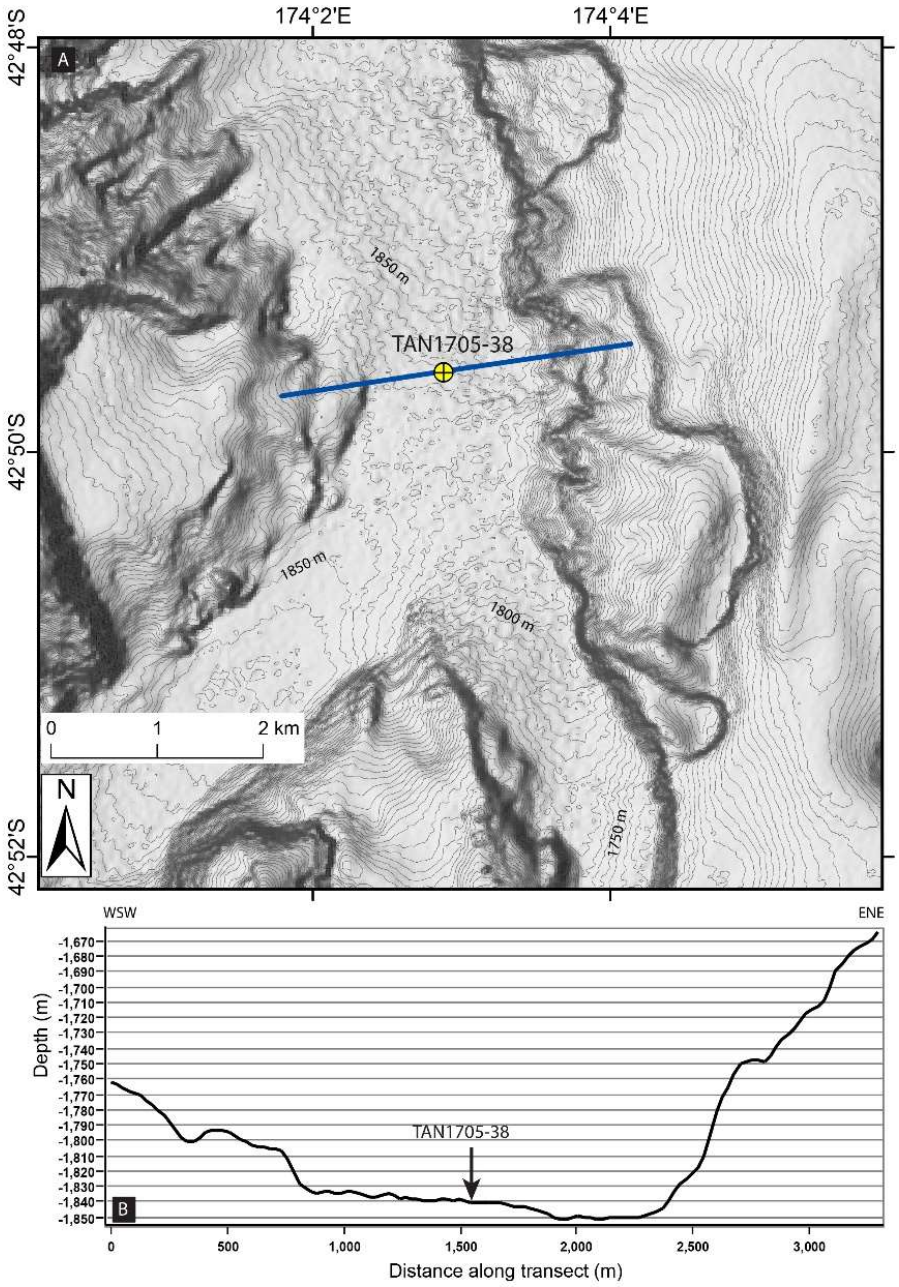

Supplementary Figure 13. Bathymetric setting of core site TAN1705-38

Lat. -42.8268, Long. 174.0480. Water depth 1838 m.

Presence of 2016 M_w 7.8 Kaikōura earthquake turbidite: No.

a, Bathymetric map derived from SIMRAD Kongsberg EM302 multibeam data gridded to 25 m, showing bathymetric contours at 5 m intervals draped over a multi-directional hillshade with vertical exaggeration of 2. Multicore TAN1705-38 is located on the continental slope off northeastern South Island, in the lower reaches of Pegasus Canyon. The core is positioned to within an accuracy of 10 m, using an ultra-short baseline (USBL) underwater acoustic positioning system on R.V. *Tangaroa*. The site lies about 2 km downstream of the confluence between the Pegasus and Pūkākī canyons, where the channel is about 1.4 km wide. **b,** Bathymetric cross-section showing the site is located in the centre of the channel, 10 m above the maximum channel depth.

Supplementary Discussion 1 - Age of the turbidite

Multiple lines of evidence support very recent emplacement of the turbidites that we infer were formed in response to the Kaikōura earthquake. Excess ^{234}Th was measured in cores TAN1613-53 from the Hikurangi Trough (Fig. 1) and TAN1613-52 from the Hikurangi Channel[2]. Activities of 100-150 Bq.kg^{-1} of excess ^{234}Th were present in turbidite sediments, while the highest level of excess ^{234}Th activity of 480 Bq.kg^{-1} was detected in the oxic layer immediately beneath the turbidite[2] (Supplementary Fig. 14a). High levels of excess ^{234}Th activity in the turbidite sediment and the underlying oxidized layer provide unequivocal evidence of recent emplacement. At the time of coring (3 days after the 2016 Kaikōura earthquake) turbidites were highly fluidized, suggesting the deposit was still settling[2]. Additionally, fresh biological remains were identified in turbidite sediments from the Hikurangi Channel, lending further support for deposition immediately prior to coring[2].

Sedimentary evidence that supports emplacement of new turbidites include burial of the reddish brown oxic layers underlying the deposits, at locations where the turbidity current has not eroded the seafloor. These oxic layers are characteristic of an un-disturbed seafloor where sediments have been at the sediment-water interface and subject to biological activity for extended periods[3]. Oxic layers occur at the sediment water interface in pre-Kaikōura earthquake cores, but are absent from the sediment water interface of 2016 Kaikōura turbidites (Supplementary Fig. 14c). The turbidites also exhibit evidence of rare bioturbation, in contrast with the highly bioturbated underlying sediments (Supplementary Fig. 14a,b). The relative lack of bioturbation suggests insufficient time has elapsed following turbidite deposition to allow for colonisation and reworking of the sediments by benthic organisms. The utility of the degree of bioturbation as a proxy for recent deposition is provided by the quantifiable increase in bioturbation of the 2016 Kaikōura turbidite seen in cores TAN1613-53 and TAN1705-21 from the same Hikurangi Trough site, but collected 8 months after the event (Supplementary Fig. 14a,b). Despite these rapid bioturbation rates, the 2016 Kaikōura deposit remains easily distinguishable and less bioturbated than the underlying older turbidites (Supplementary Fig. 14).

Evidence of the recent deposition of the 40 cm thick turbidite at site TAN1705-27, located in the axis of the Cook Straight Canyon, was also established by repeat coring. This site was first cored on 11 November 2016, several days before the 2016 Kaikōura earthquake and then again 8 months later on 5 May 2017. The absence of the 40 cm turbidite in the pre-earthquake core supports the 2016 Kaikōura earthquake origin of this bed.

Preliminary measurements of ^{210}Pb activity in cores from TAN1705 26 and TAN1704 24 show exponential decays in activity down core from under the 2016 Kaikōura turbidite (Supplementary Figure 15). These decreases in ^{210}Pb activity with depth are indicative of excess ^{210}Pb being present in the sediments. We cannot directly quantify excess ^{210}Pb with the existing data because the samples do not extend deep enough into the cores to allow supported ^{210}Pb produced by decay of ^{226}Ra in the sediment to be estimated reliably. None the less, given the relatively homogenous grainsize and sediment composition below the turbidites, supported ^{210}Pb activates must be equivalent to or lower than the measured ^{210}Pb values obtained from the deepest core samples i.e. <50 Bq.kg^{-1}. This is an important observation because it indicates that there is excess ^{210}Pb in the sediments that immediately underlie the 2016 Kaikōura turbidite in both cores and potentially in the turbidites themselves. ^{210}Pb has a half-life of 23 years and excess ^{210}Pb is unlikely to persist in sediments that were deposited more than 100 years ago on the Hikurangi Margin[4]. Hence, the presence of excess ^{210}Pb in sediments underlying the surficial turbidites show they were deposited within the last century. The high ^{210}Pb activity in the oxic sediments below the surficial turbidite in TAN1705 24 provides further evidence of recent deposition. While the sedimentological evidence of very recent deposition provides the strongest rationale that these turbidites were triggered by the 2016 Kaikōura earthquake, the ^{210}Pb data eliminates the last major earthquake to occur on the HSM which was the 1855 M_w8.2 Wairarapa earthquake[5].

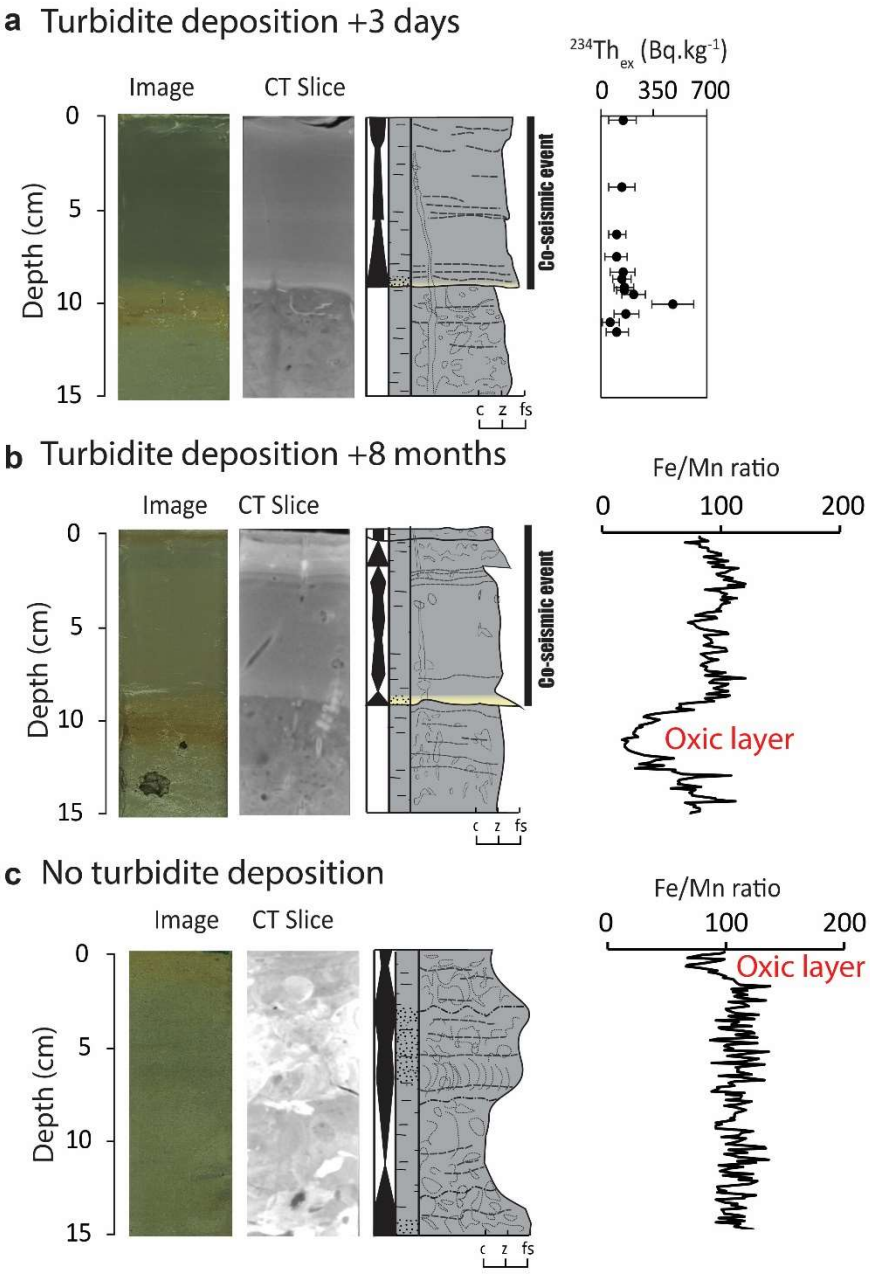

Supplementary Figure 14: Repeat coring at the Hikurangi Trough site. a, Core top turbidite in a core taken 3 days after the 2016 Kaikōura earthquake. The 2016 Kaikōura turbidite overlies an oxic pre-earthquake sea floor and excess ^{224}Th activity profiles confirm very recent deposition. **b,** Core top turbidite in a core taken 8 months after the 2016 Kaikōura earthquake. **c,** Highly bioturbated pre-Kaikōura core top turbidite with oxic layer developed at the sediment-water interface, as shown by the decrease in the Fe/Mn ratio from core site TAN1705-22. Quantifiable bioturbation of the 2016 Kaikōura event bed has occurred in the 8 months since deposition indicating that bioturbation rates are rapid. Grainsize scale is: c – clay; z – silt; and fs- fine sand.

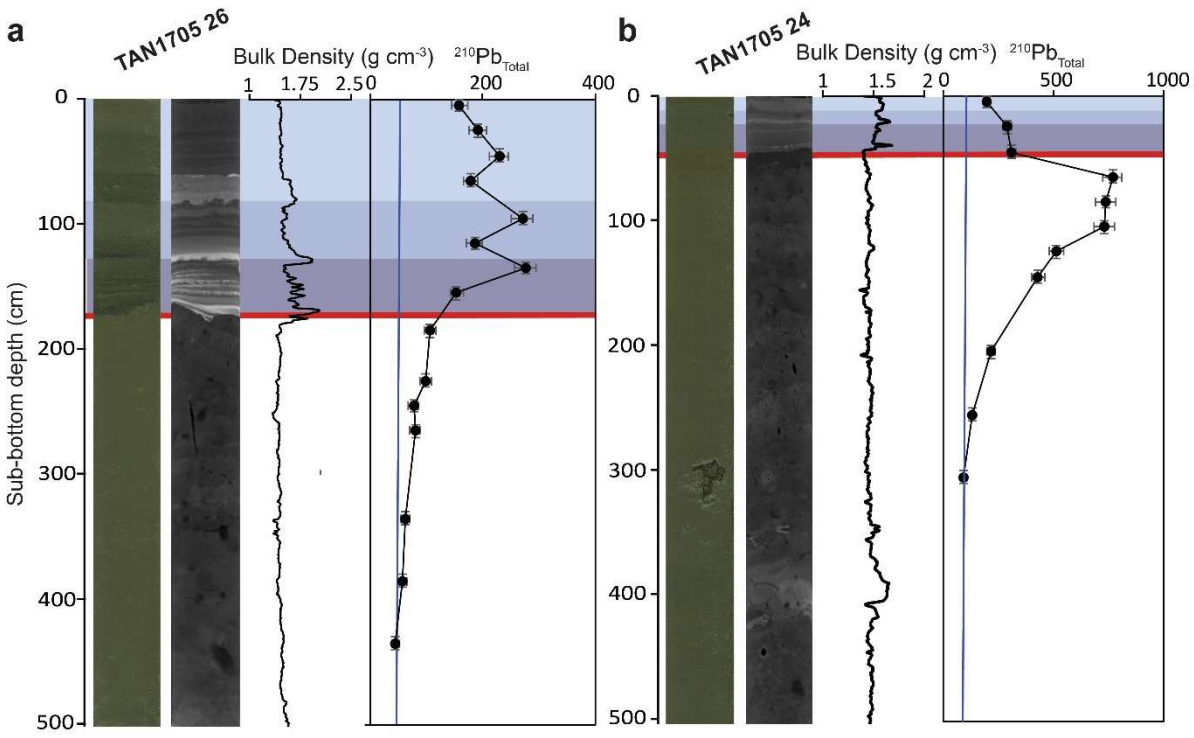

Supplementary Figure 15: Total ^{210}Pb activities in the 2016 Kaikōura earthquake turbidite and underlying sediments from TAN1705 26 (a) and TAN1705 24 (b). Blue vertical lines represent the inferred maximum possible supported ^{210}Pb activity; the horizontal red line represents that based of the 2016 Kaikōura turbidite; vertical blue bands present grainsize pulses in the turbidites.

Supplementary Discussion 2 - 2016 Kaikōura turbidite lithofacies

The set of 23 cores provides insights into the presence/absence of deposits from the 2016 Kaikōura earthquake triggered turbidity currents, and informs the spatial extent of triggering in discrete canyons along the Hikurangi Subduction Margin (HSM).

Turbidites deposited by the 2016 Kaikōura earthquake range in thickness from 20–650 mm (Fig. 1a). The thickest turbidites associated with the 2016 Kaikōura earthquake occur in the thalweg of the Hikurangi Channel, >680 km north of the source area[2]. In the southern canyons, the turbidites are all less than 50 mm thick (Fig. 2), while in the northern canyons they range from 20–400 mm thick (Fig. 2). Turbidite thickness in the northern canyons decreases from South to North along the margin (Fig. 2).

The stratigraphy of the turbidites deposited by the 2016 Kaikōura earthquake turbidity currents varies in complexity from south to north along the spatial extent of triggering (Fig. 2). In the three southern-most canyons turbidites are characterised a ~5 mm thick basal lamination of very fine sandy silt (T_D) that is overlain by a normally graded, massive silty mud (T_{E-2}) that has a sharp, flat-lying lower contact (Supplementary Fig. 15a; Supplementary Table 2). These T_D–T_{E-2} beds are interpreted to have formed by deposition from a waning turbidity current. Put another way, the turbidites are interpreted to have formed by a turbidity current with a single velocity surge.

2016 Kaikōura turbidites in the more northern canyons are characterised by greater bed and sedimentary structure complexity. They are composed of two to five stacked, normally graded bands (i.e. thicker than laminations, but all within a single bed), each separated by sharp, sometimes loaded contacts (Supplementary Fig. 15b). Each normally graded band is characterised by 5–50 mm of planar laminated, very fine, sandy silt (T_D) that grades into 5–100 mm of planar laminated and normally graded mud (T_{E-1}) or massive and normally graded mud (T_{E-2}). A notable exception to this is core TAN1705 27 from the axis of the Cook Straight Canyon (the largest canyon system in the HSM). Here, a 40 cm thick pebble grain sized turbidite is observed. It is considerably coarser (up to small pebbles) than the other silt-dominated turbidites described herein (Fig. 2). Despite the variation in texture, the Cook Strait Canyon turbidite is still comprised of between two to five normally graded bands separated by sharp contacts (Fig. 2). The lower most sequences are composed of planar banded, very fine pebbly, coarse to medium sand (T_{B-1}), overlain by convoluted silty, fine sand bands and laminae that are rich in shell fragments (T_C). The uppermost, normally graded sequence has a basal band of planar bedded, fine sand (T_D), separated from the overlying normally graded mud (T_{E-2}) by a sharp contact. The presence of low density shell-hash layers in the T_C bands obscure the relationship between density and grainsize observed in other cores. For example, the density trough

at 200 mm on the TAN1705 27 core appears to be an artefact of the loosely consolidated shell hash rather than a reduction in grainsize. Hence, on the basis of the density grainsize proxy it is difficult to determine exactly how many grainsize pulses there are in the turbidite, but it could range from between two to five (Fig. 2).

The stacked set of multiple normally graded bands in the majority of turbidites from the northern canyons is interpreted to be deposited by turbidity currents that has multiple distinct velocity surges.

As noted above, cores that lack lithological evidence of a recently deposited turbidite have core tops characterised by heavy bioturbation and the presence of a reddish brown oxic layer at the sediment water interface (Supplementary Fig. 14c).

Supplementary Table 2: Description of core lithofacies from the canyons and slope basins cored in this study.

Lithofacies*	Description	Interpretation
T_{B-1}	Up to 100 mm thick beds of planar laminated coarse to medium sand.	Formed by reworking of coarse to medium sand grains as bedload beneath a low density turbidity current.
T_C	Up to 100 mm thick beds of convoluted silty, fine sand bands and laminae .	Formed by reworking of medium to fine sand grains as bedload beneath a low density turbidity current.
T_D	Up to 50 mm thick beds of planar bedded, fine sand and very fine sandy silt.	Formed by reworking of very fine sand and coarse grains as bedload beneath a low density turbidity current.
T_{E-1} and T_{E-2}	Up to 100 mm thick, planar bedded, or normally graded mud.	Formed by settling from a low density turbidity current.

*Turbidite classification after Talling et al.[6].

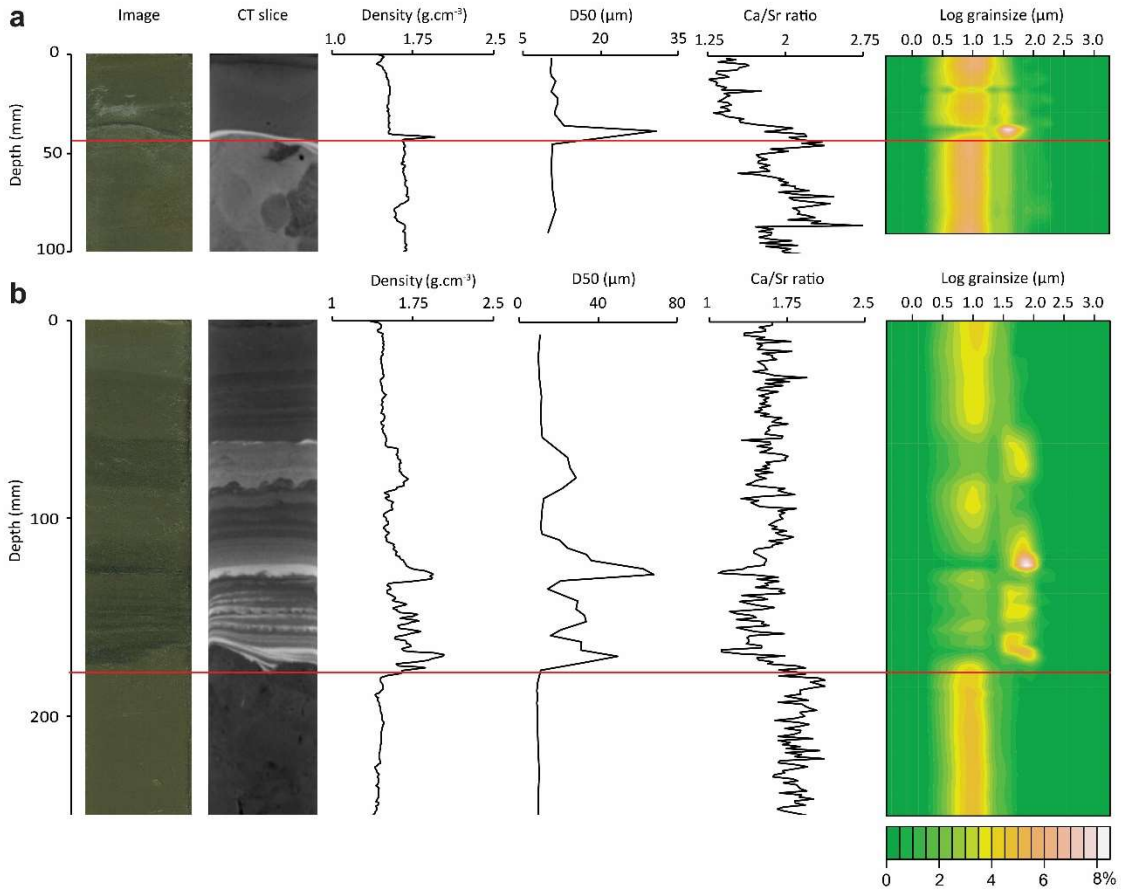

Supplementary Figure 16: The relationship between grainsize and bulk density derived from CT tomography. **a,** Linescan image, CT tomography sagittal slice, bulk density, grainsize D50, Ca/Sr ratio and grainsize heat map for TAN1705 36, a representative core for single-banded turbidite character from the southern canyons. **b,** Linescan image, CT tomography sagittal slice, bulk density, grainsize D50, Ca/Sr ratio and grainsize heat map for TAN1705 26, which is a representative core for the multi-pulse turbidites from the northern canyons. Bulk density correlates very well with D50 in both simple and complexly bedded turbidites.

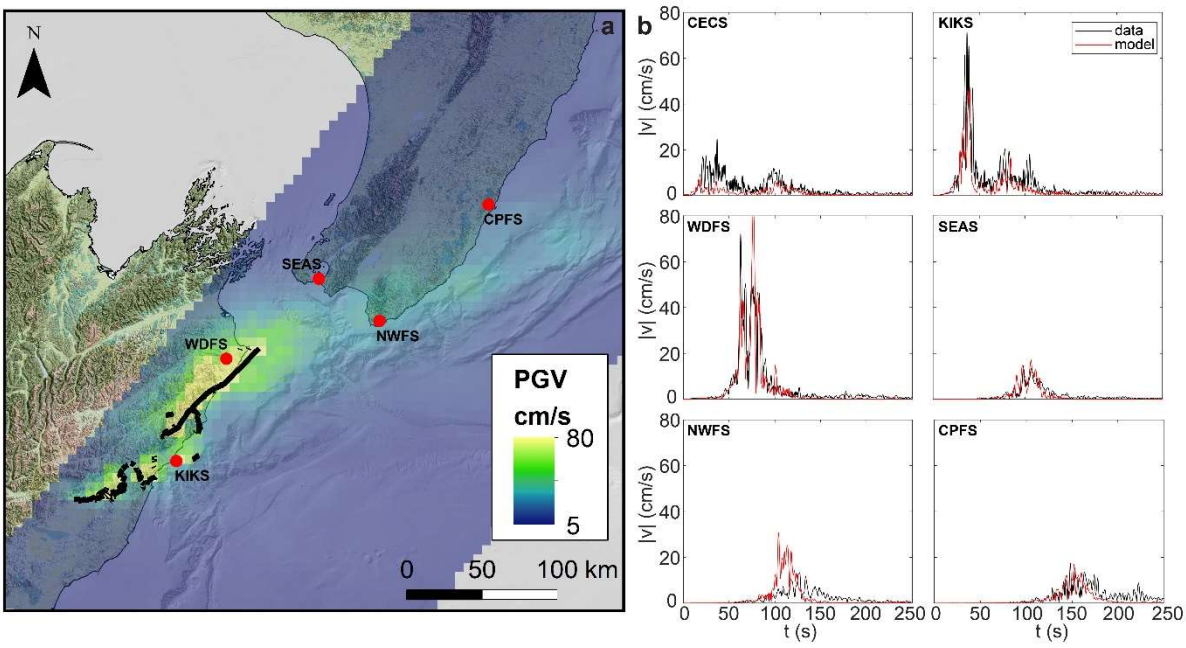

Supplementary Figure 17: Physics-based simulation of strong ground motions generated by the 2016 Kaikōura earthquake. a, Peak Ground Velocity (PGV) is shown along the southern Hikurangi Margin. **b,** The model shows excellent agreement with measured velocity time histories from seismic stations located along the length of the margin. Black line shows the fault rupture during the 2016 Kaikōura earthquake.

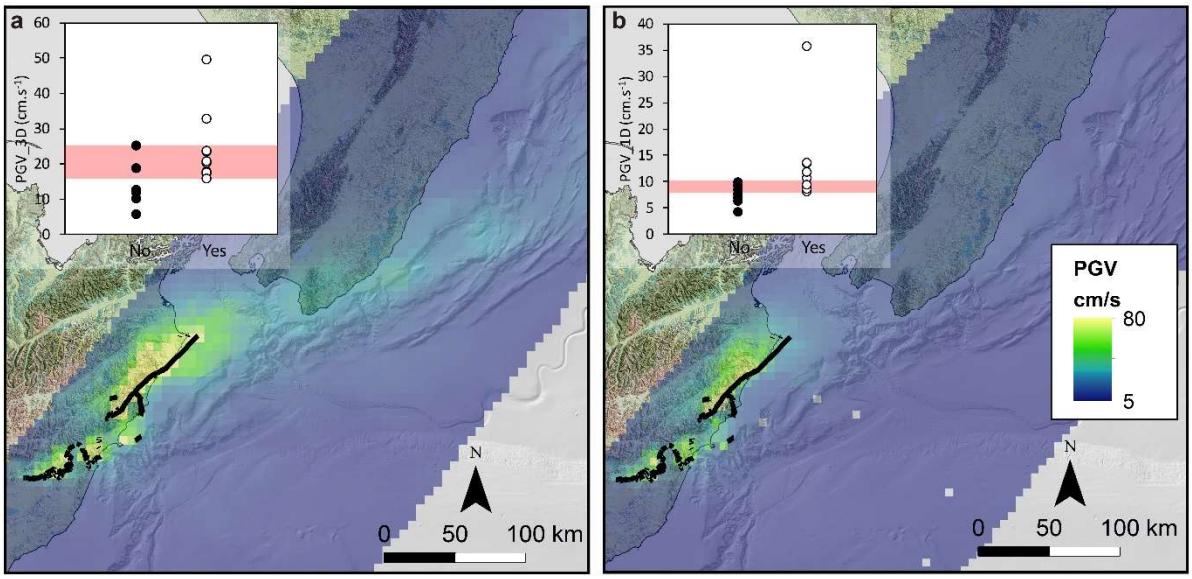

Supplementary Figure 18: **Comparison of simulated peak ground velocities for the 2016 Kaikōura earthquake.** The simulations are produced with **a**, the 3D velocity model and **b,** the 1D, layered velocity model.

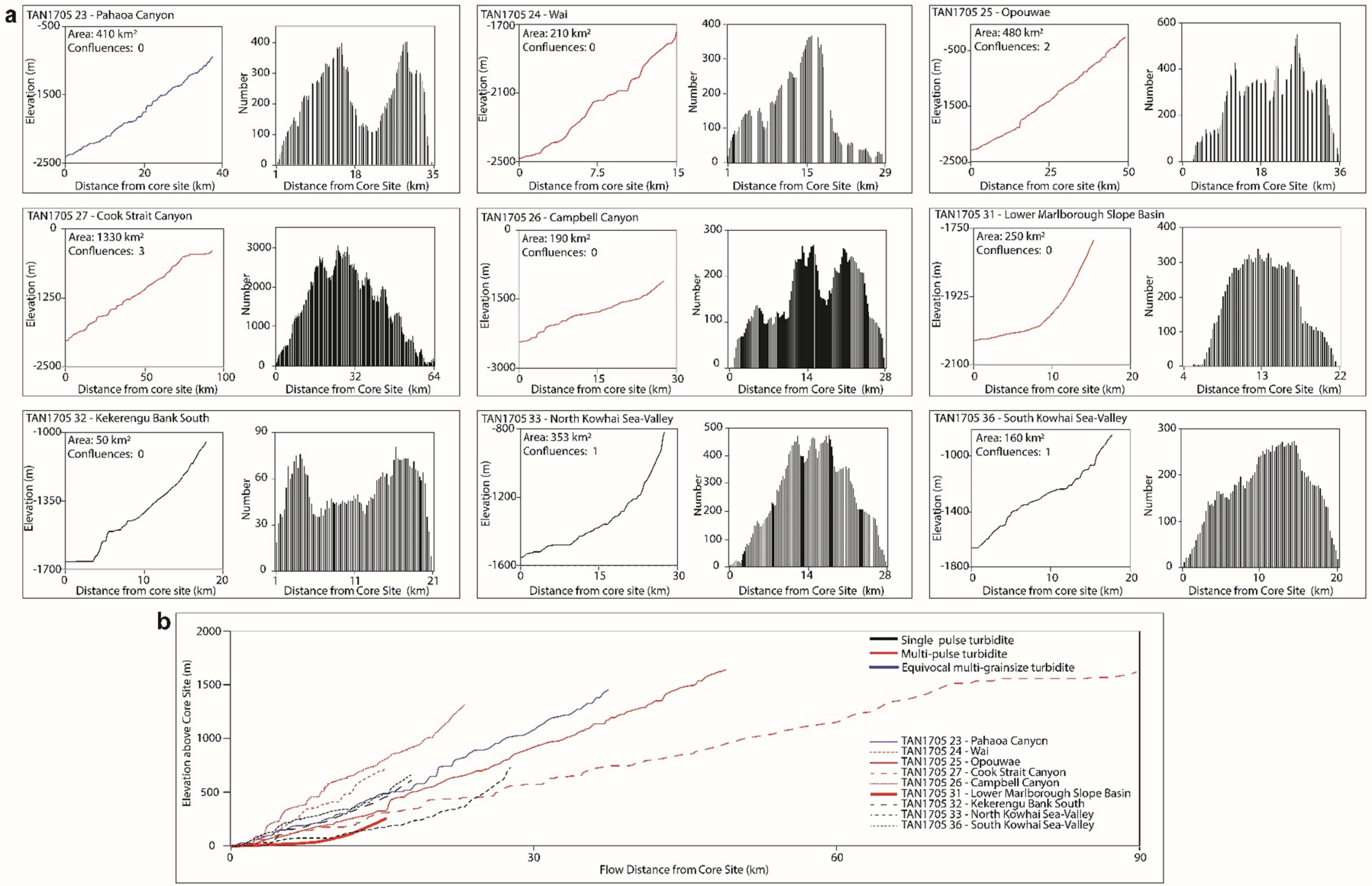

Supplementary Figure 19: Morphometric analysis of the canyons that had turbidites emplaced by the 2016 Kaikōura earthquake. a, Plots showing the gradient of the maximum thalweg distance and histogram of flow path distance from source areas to the core site for all canyons that had a coseismic turbidite emplaced by the Kaikōura earthquake. **b,** Gradients of the maximum thalweg distance for the canyons on a normalised elevation above core site. Red lines – core sites that have multi-pulse turbidites; blue line – equivocal multi-pulse turbidites; and black lines – single pulse turbidites. Canyon area, thalweg gradient, average flow path distance and number of major confluences do not vary systematically between canyons that have a single vs multi-pulse turbidites.

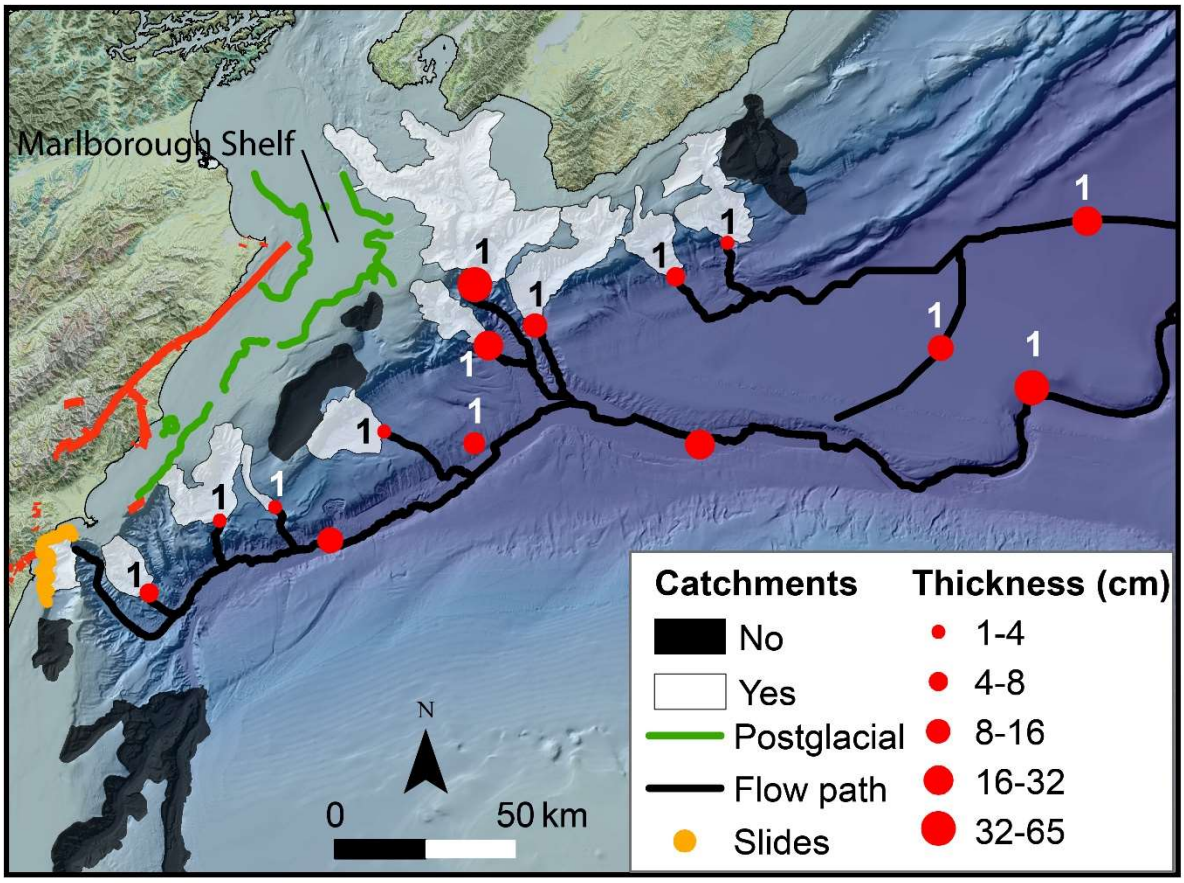

Supplementary Figure 20: Count of turbidites deposited by the 2016 Kaikōura earthquake up- and downstream of major channel and canyon confluences. A single turbidite was identified up- and downstream of all major flow path confluences demonstrating coherent triggering of turbidity currents in adjacent canyons and evolution of these currents into a long run out flow. Core sites marked with red dots without the number 1 preserve evidence for the 2016 Kaikōura earthquake turbidite but the core did not sample the underlying sediments and therefore it is not possible to assess the number of turbidites at these locations. Green lines represent the 0 m sediment isopach thickness for post-last glacial (<20 kyr) deposits on the eastern Marlborough continental shelf. The seaward edge of the deposit does not extend east to the shelf break, where there are structurally-uplifted mid Pleistocene or older units outcropping at the seafloor[7]. The consolidation state of the sediments in the head of the adjacent upper-slope gully may provide an explanation why no turbidity current was triggered there by the 2016 Kaikōura earthquake.

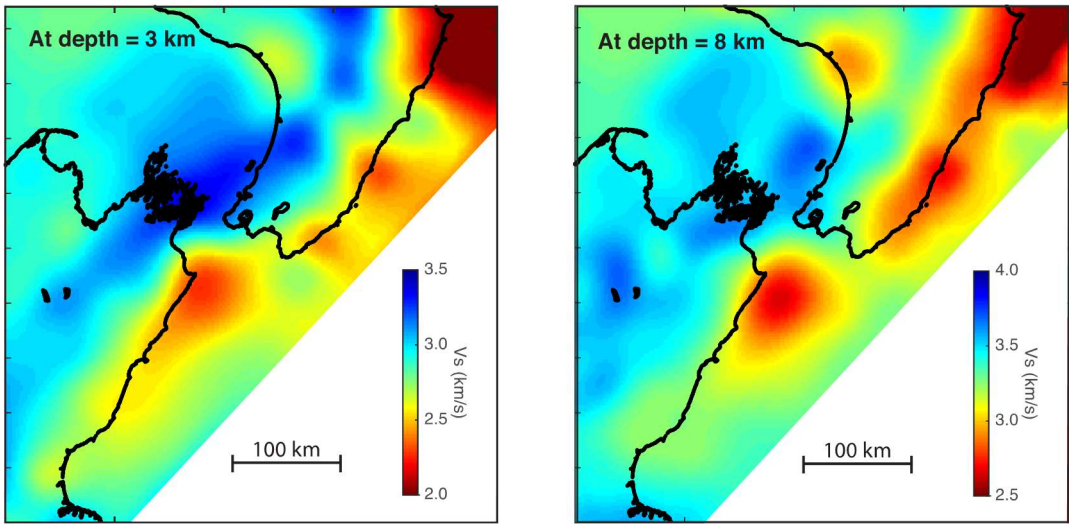

Supplementary Figure 21: Map of shear-wave velocity (Vs) at 3-km and 8-km depths in the velocity model. The offshore velocity is constrained by onshore-offshore data from marine air-gun shots recorded at onshore station[8].

Supplementary Discussion 3 - Slope failure triggering mechanisms

A plausible explanation for the seafloor failure mechanism resulting in a link between the earthquake ground motion-time history and multi-pulsed turbidites is shallow retrogressive landslide failure during the shaking period. The presence excess ^{210}Pb in multi-pulsed turbidites (Supplementary Figure 15) indicates failure of recent and therefor shallow sediments, which is in agreement with other regional seismic triggering of landslides[2,9]. Failure of weak unconsolidated surface sediments during the initial seismic perturbation would reduce the stability of sediments upslope even further leading to failure in subsequent ground motion peaks.

A shallow translational slab mechanism of failure is likely here, as the sediment is fine grained and likely to resist liquefaction failure. In laboratory experiments, episodes of high-intensity ground motion during an earthquake can be correlated, in time, with the displacement and failure of slopes[10,11]. Hence, we suggest the following multi-stage failure model:

1. The first interval of high-intensity ground motion (high amplitude velocity peak) fails a portion of the submarine slope (mass 1) where the factor of safety is lowest (as a function of slope gradient, material properties etc.). This weak failed sediment evolves into a downslope sediment flow and will form the first grainsize pulse in the downstream turbidite.

2. The headscarp behind failure mass 1 has removed lateral support from the slope above reducing the factor of safety and is subjected to a further peak in high intensity shaking, causing failure of this "mass 2". This material flows downslope to become the second grainsize pulse in the downstream turbidite.

4. Step 2 is repeated for subsequent high amplitude ground motion peaks.

Another potential contribution to a cyclic process of slope failure is surface-sediment remobilisation that is inferred to occur when earthquake ground motions induce transient stresses at the sediment-water interface. These can cause remoulding and localised excess pore pressures in the very water-rich, weak and unconsolidated surficial sediment[3,12,13,14]. The shear strength reduction associated

with the excess pore pressures and remoulding allows the surficial sediment to move downslope[13]. In these saturated, under consolidated and hence weak sediments the transient increases in pore pressures are likely to be co-temporal with amplitude peaks in ground motions[15], potentially providing discrete episodes of failure that could produce turbidity currents with multiple velocity surges. We acknowledge that the hypothesised seafloor failure mechanisms remain highly speculative without detailed radiometric analysis of source area sediment, information on the geotechnical properties of the sediments in sources areas and observations of morphological change after the earthquake. Testing the plausibility of these failure mechanism should be the focus of future work.

References:

1 Meng, Q., Ni, S., Guo, A. & Zhou, Y. Ground Surface Deformation Caused by the Mw 5.8 Early Strong Aftershock following the 13 November 2016 Mw 7.8 Kaikōura Mainshock. *Seismological Research Letters* **89**, 2214-2226, doi:10.1785/0220180019 (2018).

2 Mountjoy, J. J. *et al.* Earthquakes drive large-scale submarine canyon development and sediment supply to deep-ocean basins. *Science Advances* **4**, doi:10.1126/sciadv.aar3748 (2018).

3 McHugh, C. M. *et al.* Remobilization of surficial slope sediment triggered by the A.D. 2011 Mw 9 Tohoku-Oki earthquake and tsunami along the Japan Trench. *Geology* **44**, 391-394, doi:10.1130/g37650.1 (2016).

4 Alexander, C. R., Walsh, J. P. & Orpin, A. R. Modern sediment dispersal and accumulation on the outer Poverty continental margin. *Marine Geology* **270**, 213-226, doi:https://doi.org/10.1016/j.margeo.2009.10.015 (2010).

5 Downes, G. & Dowrick, D. Atlas of isoseismal maps of New Zealand earthquakes-1843-2003 Second edition (revised) (GNS Science, Lower Hutt, 2014).

6 Talling, P. J., Masson, D. G., Sumner, E. J. & Malgesini, G. Subaqueous sediment density flows: Depositional processes and deposit types. *Sedimentology* **59**, 1937-2003, doi:10.1111/j.1365-3091.2012.01353.x (2012).

7 Barnes, P. M. & Audru, J. C. Quaternary faulting in the offshore Flaxbourne and Wairarapa Basins, southern Cook Strait, New Zealand. *New Zealand Journal of Geology and Geophysics* **42**, 349-367, doi:10.1080/00288306.1999.9514851 (1999).

8 Eberhart-Phillips, D. & Bannister, S. 3-D imaging of the northern Hikurangi subduction zone, New Zealand: variations in subducted sediment, slab fluids and slow slip. *Geophysical Journal International* **201**, 838-855, doi:10.1093/gji/ggv057 (2015).

9 Mosher, D. C. & Piper, D. J. W. in *Submarine Mass Movements and Their Consequences: 3 International Symposium* (eds Vasilis Lykousis, Dimitris Sakellariou, & Jacques Locat) 77-88 (Springer Netherlands, 2007).

10 Wartman, J., Bray, J. D. & Seed, R. B. Inclined Plane Studies of the Newmark Sliding Block Procedure. *Journal of Geotechnical and Geoenvironmental Engineering* **129**, 673-684, doi:doi:10.1061/(ASCE)1090-0241(2003)129:8(673) (2003).

11 Wartman, J., Seed, R. B. & Bray, J. D. Shaking Table Modeling of Seismically Induced Deformations in Slopes. *Journal of Geotechnical and Geoenvironmental Engineering* **131**, 610-622, doi:doi:10.1061/(ASCE)1090-0241(2005)131:5(610) (2005).

12 Molenaar, A., Moernaut, J., Wiemer, G., Dubois, N. & Strasser, M. Earthquake Impact on Active Margins: Tracing Surficial Remobilization and Seismic Strengthening in a Slope Sedimentary Sequence. *Geophysical Research Letters* **46**, 6015-6023, doi:10.1029/2019gl082350 (2019).

13 Moernaut, J. *et al.* Lacustrine turbidites produced by surficial slope sediment remobilization: A mechanism for continuous and sensitive turbidite paleoseismic records. *Marine Geology* **384**, 159-176, doi:10.1016/j.margeo.2015.10.009 (2017).
14 Schwestermann, T. et al. Multivariate Statistical and Multiproxy Constraints on Earthquake-Triggered Sediment Remobilization Processes in the Central Japan Trench. Geochemistry, Geophysics, Geosystems **21**, e2019GC008861, doi:https://doi.org/10.1029/2019GC008861 (2020).
15 Biscontin, G., Pestana, J. M. & Nadim, F. Seismic triggering of submarine slides in soft cohesive soil deposits. *Marine Geology* **203**, 341-354, doi:https://doi.org/10.1016/S0025-3227(03)00314-1 (2004).